Universitetet i Stavanger

Faculty of Science and Technology

MASTER'S THESIS

Study program/Specialization: Petroleum technology	Spring semester, 2016 Open
Writer: Maren Louise Boiten	…… (Writer's signature)

Faculty supervisor:

Professor Rune Wiggo Time

Co-Supervisor:

Milad Khatibi

Hermonja A. Rabenjafimanantsoa, Benja

Thesis title

Experimental study on cuttings transportation in turbulent pipe flow

Credits (ECTS):

30

Key word: Particle transport Pressure drop Flow patterns Velocity profile Rotating drill string	Pages: 86 + enclosure: 3 Stavanger, 15.06.2016

Experimental study on cuttings transportation in turbulent pipe flow

Maren Louise Boiten

University of Stavanger

June 2016

Preface

This master thesis is written based on earlier studies done at the University of Stavanger and as a small part of a PhD study on multiphase flow in pipes. This master thesis is weighted with 30 credits.

I am grateful for getting the opportunity to write this thesis for Professor Rune W. Time at the University of Stavanger and for using the multiphase lab as well as Professors Times personal equipment. His feedback and knowledge has been very helpful.

I would like to express my deepest appreciation to Milad Khatibi (PhD) for the time he consecrated to my work, for good guidance, for ideas on how to solve problems on the way, as well for his enthusiastic encouragement. I am also grateful for all the time he has used to develop my understanding of the subject and for providing me with MATLAB scripts.

Thanks to Senior Engineer Hermonja A. Rabenjafimanantsoa, Benja, for keeping me motivated, giving me comments as well as creating a good working atmosphere at the lab.

Finally, I will give a special thanks to Family and friends, for keeping up with me during this period.

Abstract

Experimental investigation on cuttings transportation in turbulent flow, in both horizontal and inclined pipes were performed in the multiphase-laboratory at the University of Stavanger. Spherical glass particles were used to indicate the cuttings transportation. The focus of the experiments was to investigate how pipe inclination, flow rate, particle size and rotation on drill string (DS) affect the particle transport. Different experiments were conducted for single-phase water flow and two-phase liquid-particle flow. A medium-scale flow loop was carried out to run different cases of fluid velocity at different inclinations, with and without DS. The pipes in the flow loop were transparent for better visualization of the flow patterns and measuring the liquid and particle velocity profiles. Both the particle image velocimetry (PIV) and ultrasonic velocity profile (UVP) measurement techniques were applied. The results showed that the different pipe inclinations influenced on particle flow patterns. At higher pipe inclination, the transitions in flow patterns were occurring at lower superficial liquid velocity (Usl). The flow patterns were also affected by the rotation of DS. The rotation of DS caused the particles to be distributed more uniformly in the cross section, which gave a positive impact on the particle transport. The velocity profiles measured by PIV indicated the effect of different parameters like rotation of DS. However, the velocity profiles measured by PIV and UVP were in good agreement.

Contents

Nomenclature

Greek symbols

θ_{trans}	Angle on the transducer
$\Delta\bar{x}$	Particle displacement
Δt	Amount of time
ΔP	Differential pressure
μ	Fluid viscosity [$kgm^{-1}s^{-1}$]
ε	Relatively roughness
θ	Angle on the test section
λ	Ultrasonic wave length [$ms^{-1}Hz^{-1}$]
ρ	Fluid density [kgm^{-3}]
τ	Shear stress [Nm^{-2}]

Roman symbols

A	Area [m^2]
BHA	Bottom Hole Assembly
c	Speed of sound in water [ms^{-1}]
C_p	Concentration of particles
CMB	Continuing Moving Bed
D	Pipe Diameter [mm]
dl	Length on test section
DP	Differential Pressure [mbar]
DS	Drill String
dv/dy	Shear rate [s^{-1}]
$d_{Horizontal}$	Distance in horizontal direction [m]
d_{UVP}	Distance measured by the UVP [m]
d_{sp}	Seeding particle diameter [m]
d_θ	Distance in inclined pipe[m]
ECD	Equivalent Circulation Density
f	Transducer frequency [MHz]

FFT	Fast Fourier Transform
f_f	Darcy friction factor
ID	Inner Diameter [mm]
ID_{pipe}	Inner Diameter of pipe [mm]
LED	Light Emitting Diode
MB	Moving Bed
MTV	Minimum Transport Velocity
OD	Outer Diameter [mm]
OD_{DS}	Outer Diameter of "drill string" [mm]
PIV	Particle Image Velocimetry
P_H	Pressure high side [mbar]
P_L	Pressure low side [mbar]
Q_L	Liquid flow rate [m^3s^{-1}]
Q_P	Particle flow rate [m^3s^{-1}]
Re	Reynolds number
rpm	Rotation per minute
SB	Stationary Bed
SD	Standard Deviation
SEM	Scanning Election Microscope
SMB	Separated Moving Bed
u	Velocity x-direction [ms^{-1}]
U_m	Mean velocity [ms^{-1}]
Usl	Superficial velocity of liquid [ms^{-1}]
$Usl_{annulus}$	Superficial velocity in 5^0 in annulus [ms^{-1}]
Usp	Superficial velocity of particles [ms^{-1}]
UVP	Ultrasonic Velocity Profile
$u_{Horizontal}$	Velocity in horizontal direction [ms^{-1}]
u_{UVP}	Velocity measured by UVP in x-direction [ms^{-1}]
u_θ	Velocity in flow direction for inclined test section [ms^{-1}]
v	Velocity y-direction [ms^{-1}]
v_θ	Velocity in the direction 90^o from flow direction for inclined test section [ms^{-1}]
$\bar{v}$	Vector velocity [ms^{-1}]
v_{UVP}	Velocity measured by UVP in y-direction [ms^{-1}]

List of figures

List of tables

1. Introduction

In order to have a good drilling program it is essential to have good cuttings transportation. Bad cuttings transportation can lead to costly operations and is therefore unwanted. To avoid the problem with cuttings transport, it is best to keep the wellbore as near to 90^{o} from horizontal (vertical) as possible. When the angle from horizontal decreases, the particles may start to accumulate either as a stationary or as a moving bed, depending on how large the wellbore angle is. All the angles mentioned in this thesis are described from horizontal. A rotating drill string can be a solution to get good cuttings transportation in an inclined wellbore. (Nazari, Hareland, & Azar, 2010)

1.1. Aim of study

The aim of this report is firstly to study the connection between pressure drop and flow pattern due to different inclinations on the pipe and changes in flow rate. Secondly to give an indication on how a rotating Drill String (DS) with different rotation speed changes the pressure drop and the particles flow patterns at different flow rates. The pressure drop was measured for both single-phase water flow and two-phase liquid-particle flow. The measurement techniques, Particle Image Velocimetry (PIV) and Ultrasonic Velocity Profile (UVP) have been applied to give a good view of the velocity profile inside the pipe. A $25\ mm$ pipe was induced into the 5^{0}-inclined test section, to illustrate the impact of a rotating DS.

1.2. Background

During years of increased interest for directional drilling, the amount of studies in cuttings transport has increased. Still, due to the difficulties in setting up a large experimental setup, there are only a few studies done on cuttings transportation for inclined wellbores. Most of these studies have been performed in a large-scale flow loop at the University of Tulsa. Through the earlier studies, it has been discovered that rheology, inclination on the wellbores, flow rate and rotation on DS have the largest impact on cuttings transportation.

Studies done by Clark and Bickham (1994) show that inclination in a wellbore makes cuttings transport more difficult. Adari, Miska, Kuru, Bern, and Saasen (2000) found that turbulent flow

is most beneficial for inclined wellbores and that their model had to be further developed in order to conclude on the impact of a rotating DS. Pinchas Doron and Barnea (1995) concluded that the flow pattern affects the pressure drop.

H. Rabenjafimanantsoa (2007) found that the methodology could reasonably describe the understanding of liquid-particle flow. His studies were done to gain insights into the fundamental role that turbulent coherent structures plays in the incipient motion and transport of particle bed-dune in pipe flow. He looked at the pressure drop through the pipe section, total mass flow, bed heights and critical velocities.

2. Theory

This chapter gives a short description of what controls the cuttings transport and how the cuttings transport can be made as effective as possible. Conclusions from some of the earlier studies are mentioned together with an overview of information about particles behavior, pressure drop, fluid flow, flow patterns and the measurement techniques used for creating a velocity profile in this thesis.

2.1. Cutting transportation

Cuttings transportation are controlled by many different variables, such as wellbore and DS diameter, wellbore inclination, fluid velocity, rate of penetration and cutting characteristics. Bad cuttings transport can lead to slow drilling rate, lost circulation, formation fracturing because of increased Equivalent Circulation Density (ECD), bit wear, high torque, and in worst case the drill pipe can get stuck (Egenti, 2014).

Today it is known that the smaller the cuttings are, the higher flow rate is needed, to be able to transport the cuttings from the downhole and up to the surface. A high flow rate has its disadvantages because of the increase in frictional pressure drop, and can therefore results in problems like increased ECD and potential erosion in the wellbore. Rotation on the DS has also a positive impact on cuttings transportation, but this leads to induced cyclic stress, that can result in premature pipe fatigue. The rheology of the drill fluid is another parameter that can be changed to increase the cuttings transportation. The three factors, high flow rate, rotation speed on DS, and rheology are concluded to be the most effective focus areas to obtain increased cutting transport (Nazari et al., 2010).

2.1.1. Flow rate

Studies have shown that annular mud velocity has to be generally higher in directional drilling than in vertical drilling to limit cutting beds formation (Okrajni & Azar, 1986). Over the years, different methods and models have been developed to make it possible to assist in finding the Minimum Transport Velocity (MTV). The MTV is the minimum velocity of the lowest possible flow needed to transport particles. Mohammadsalehi and Malekzadeh (2011) presented a detailed combination of how Larsen's model and Moore's correlation can be used to predict

and calculate the MTV for all range of wellbore inclination from 0^0-90^0. Originally, Larsen's model can be used to find the MTV for cuttings removal in wellbores with an inclination between 0^0-35^0. Moore's model is used to find the slip velocity for cuttings in vertical wellbores (Mohammadsalehi & Malekzadeh, 2011).

2.1.2. The effect of a rotating inner pipe

A rotating DS (inner pipe) inside the pipe, leads to turbulent flow, this can prevent build-up of cutting beds and improve wellbore cleaning. The higher the number of rotations per minute (rpm) on the inner pipe, the smaller the size of the cuttings can be, to successfully be transported up to the surface. A normal range of DS rotations is around 90 to 180 rpm, depending on whether it is with or without drill bit (Egenti, 2014).

In unstable formations, high rpm values can cause serious problems like washout and damaging on the electronics part in the Bottom Hole Assembly (BHA) because of vibrations and unstable formations. The DS eccentricity has a strong influence on cuttings transport. It is very difficult to pin point the degree of eccentricity during the drilling operations and it is therefore difficult to get precise readings on the influence of the DS eccentricity on the cuttings transport (Adari et al., 2000).

Studies done by Duan et al. (2010) on horizontal wellbores, indicated that a rotating DS did not only significantly decreases cutting concentrations but also resulted in a considerable reductions in frictional pressure drop. The reason for decrease in frictional pressure drop was explained as due to reduced bed cross-sectional area and an increased open flow area. Accurate estimation of frictional pressure drop in annulus is essential when drilling, to keep the drilling fluid equivalent to circulating density. The circulating density has to fit into the gap between pore and fracture pressure, which can be quite narrow in cases with high temperature and pressure.

2.1.3. Rheology

Properties of the flowing media has an impact on the cuttings transport. A key role in cuttings transport near the horizontal wellbores is the shear stress at the bed interface. The bed interface is one of the reasons why the flow patterns and the DS have a significant impact on the cuttings transportation. Walker and Li (2000) found that the best way to pick up cuttings is with a low viscosity fluid in turbulent flow, to maximize the capacity a gel or multiphase system should be used to transport the solid out of the wellbore.

In laminar mud flow the fluids viscosity affects the particles slip velocity and therefore increase the impact on cuttings transport. For a mud in turbulent flow, the particles slip velocity only gets affected by the momentum force (Okrajni & Azar, 1986). Okrajni and Azar (1986) concluded that the transport performance of a mud flowing in a turbulent flow regime is not affected by the muds rheological properties. A Low viscosity that can promote turbulent flow is therefore preferred for inclined wellbores.

2.1.4. Inclination

The specific mechanism for cuttings transport depends on the wellbore angle. Experience has shown that deviated wellbores with hole angle around 25^0-50^0 are the most difficult angles to accomplish good cuttings transportation. For small angles, where stationary cuttings bed often occur, the transport is through a rolling mechanism. In larger angles, where saltating flow and moving beds can be formed, the transport is through a lifting mechanism. (Clark & Bickham, 1994). Li and Walker (2001) found that an angle of 30^0 need the highest MTV, here the cutting beds tends to be unstable and slide backward along the pipe. This indicated that inclination around 30^0 are the most difficult ones for hole cleaning.

Adari et al. (2000) found that for angles with an inclination between 45^0 and 90^0, laminar flow is the most beneficial, for smaller inclination (0^0-45^0) turbulent flow was preferred. Since turbulent flow is preferred for smaller angles, clear water is a good option as drilling fluid because of low flow requirements to induce the annular flow. Turbulent motions leads to an increase of frictional pressure drop, this again will cause an increased in shear stress on the surface of cuttings which results in an increase in cuttings removal (Mohammadsalehi & Malekzadeh, 2011).

2.1.5. Experimental setup for visualize cuttings transport

Different experimental setups are used to visualize cutting transport with different changes in parameters. Making a facility to run experiments on pressure drop and limit deposit velocity due to inclination is quite difficult, since long pipes are needed to investigate the fully developed flow (P Doron, Simkhis, & Barnea, 1997). Bilgesu, Mishra, and Ameri (2007) mention a lot of different sizes on the flow loops in their report. The pipes Inner Diameter (ID) varies from $0{,}12 - 0{,}22\,m$ and the length from $12 - 30{,}5\,m$. Many of the studies based on particle transport are conducted at the University of Tulsa. The flow loop at Tulsa, which is used in most of the studies related to this thesis has a large dimension. It is $30{,}5\,m$ long and has an ID of $0{,}20\,m$.

2.2. Particles

The density, size, shape and surface texture of particles affect their dynamic behavior in a flowing media. In different studies, different sizes and concentration of particles are used to indicate cuttings. To avoid problems due to sharp edges on the cuttings, spherical glass particles, with a higher density than water are often used. When the particles are not damaging/scratching the inside of the pipe, it is possible to know the roughness inside the pipe and calculate the friction factor. The Particles shape can also be shown to affect the viscosity of a slurry in theoretical calculations using different simplifications and configurations (Shook & Roco, 1991).

2.2.1. Forces

When the cuttings are transported to the surface, there are four different forces acting upon it, the gravitational force, the frictional forces, the drag and the lift force (Hyun, Subhash, & Osisanya, 2000). All of the forces are affected by the characteristics of the particles (cuttings) and the properties of the flowing media. To make it easier to understand the mechanism of cuttings transport, the forces are divided into two groups, the depositional- and the transport forces. These two groups are then divided into smaller groups (Egenti, 2014).

- Depositional forces:
    - The gravitational forces makes the cuttings settle down and form beds.
    - The frictional forces are the forces that occur when fluid layers and material elements are sliding against each other. The forces act against the cuttings movement.
- Transport forces:
    - The lift forces lift up the cuttings and transport it with the flow stream.
    - The drag forces rolls the cuttings out of the beds to move them forward due to viscous fluid flow over the upper exposed surface of the cuttings. These forces acts against the depositional forces.

Cuttings can be lifted in the direction normal to the flow, when the lift force is strong enough to overcome the gravitational force component. A reduction in deviated angle of the wellbore gives a decrease in drag and lift force due to an increase in gravitational force (Hyun et al., 2000)

2.2.2. Beds of particles

To get the best particles transport rate possible, dune formation should be avoided. Dunes appear most frequently in horizontal or near horizontal pipes and annulus. Once beds of particles are accumulated, they are difficult to remove. Beds of particles are formed at low flow velocities, typically in the range of $0{,}2 - 0{,}5\ m/s$ (H. A. Rabenjafimanantsoa, Time, & Saasen, 2005).

Previous studies done on two-phase liquid–particle flow in pipes, have shown development of dunes. The dunes apply a significant influence on the flow process, such as friction pressure drop, erosion and deposition (Best & Kostaschuk, 2002). H. A. Rabenjafimanantsoa et al. (2005) concludes that relations between Differential Pressure (DP) and flow velocity is an important tool for identification of flow patterns.

2.2.3. Particle-particle interaction

Particle-particle interaction controls the motion of particles in dense liquid-particle flow. As the particle concentrations becomes higher, particles collide with each other and the loss of particles kinetic energy due to inter-particle collisions can not be neglected. In multiphase flow dynamics, two phenomena are identified (Crowe, Schwarzkopf, Sommerfeld, & Tsuji, 2011):

- Collisions, merely contact with short time duration.
- Contact, contact over a longer time duration.

2.2.4. Particle-wall interaction

Analyzing the particle-wall interaction when a two-phase, liquid-particle flows is flowing inside a pipe is challenging. The particle-wall interaction falls into two categories: hydrodynamic interaction due to the proximity of a wall and mechanical interaction caused by contact with the wall. An example of the hydrodynamic interaction is the lift force that occurs due to velocity gradient near the wall. The hydrodynamic interaction can be neglected, if the particle inertia force is so strong that the collision takes place in a time much shorter than the hydrodynamic relaxation time of the particle (Crowe et al., 2011).

When a massive particle collides with a wall, it rebounds with less kinetic energy, due to friction and inelasticity effects. For very small particles approaching a wall, the molecular forces becomes dominant compared to the inertial forces. As a result, the small particles are captured on the wall, due to the cohesive forces. The cohesive force is identified as “the van der Waals force” and it prevents particles from falling down or sliding along the wall (Crowe et al., 2011).

2.3. Pressure drop in pipes

To determine the pressure drop in a pipe, knowledge of the friction between the fluid and pipe is required. When the pipe has no change in size (diameter or length) or inclination and there is only a single-phase flow inside, the only reason for pressure drop is due to friction between fluid and the pipe wall. In general, friction factor is used to determine the pressure drop. There are two ways to find the Darcy friction factors, either by using the appropriate friction factor correlation, or by reading from a Moody Chart. The methods used to find the Darcy friction factor depends on whether the flow is laminar or turbulent. In a laminar flow regime the Darcy equation may be used to determine the friction factor and in the turbulent flow regime there are many different options. The Colebrook equation is preferred, but needs to be solved iteratively to find the Darcy friction factor. Haaland, on the other hand, is an approximation of the Colebrook equation without iterations. In the transitional flow regime it is impossible to predict the friction factor because the flow pattern is inconsistent (Neutrium, Web-2012).

Pinchas Doron and Barnea (1995) showed that the flow patterns affect the pressure drop in the pipe, and this showed that the flow patterns had different pressure drops. They discovered that the earlier conclusions made in this field between stationary bed flow patterns and the flow rates at minimal pressure gradient were in most cases wrong. The minimum pressure drop had nothing to do with the transition flow rates, as Wasp et al. claimed in 1970 (P Doron & Barnea, 1996).

2.3.1. Haaland equation

The Haaland equation is an approximation of the implicit Colebrook equation. The Colebrook equation expresses the Darcy friction factor, f_f as a function of Reynolds number, Re and pipe relatively roughness, ε and can be used to find the friction factor. The Haaland equation is simple and can be easily used to find the Darcy friction factor for a full-flowing circular pipe with a given diameter, D. Even though Halland is an approximation the discrepancy from experimental data is well within accuracy of the data (Haaland, 1983). The Haaland equation is given by:

$$\frac{1}{\sqrt{f_f}} = -1{,}8log_{10}\left[\left(\frac{\varepsilon/D}{3{,}7}\right)^{1{,}11} + \frac{6{,}9}{Re}\right] \tag{2.1}$$

2.3.2. Reynolds number (Re)

Re is defined as the ratio between the inertial and the viscous forces. When the Re increases flows are characterized by regions of fast velocity variations and the occurrence of vortexes and eddies. For a flow around a circular cylinder, the Re is represented by:

$$Re = \frac{\rho u D}{\mu} \tag{2.2}$$

Where ρ is the density of the fluid, u is the inlet velocity of the flow, D is the diameter of the pipe and μ is the viscosity of the fluid (Menge, 2015).

2.4. Fluid flow

Fluid is the common term for liquid and gas. Weather a fluid is Newtonian or not, depends on if it obeys the Newton law of viscosity (eq.2.3) or not. Here τ stands for the shear stress, μ for the viscosity of the fluid and dv/dy for the shear rate, rate of strain or velocity.

$$\tau = \mu dv/dy \tag{2.3}$$

When a fluid is flowing in a pipe, the state of the flow depends on the Re. Low Re (< 3000) indicates laminar, which corresponds to slow viscous flow where frictional forces are dominant. High Re (> 4000) indicates turbulent flow (Menge, 2015). The type of flow occurring in a pipe affects the mass transport. Since Adari et al. (2000) found that turbulent flow is most beneficial for inclined wellbores, only turbulent flow is used in this thesis.

2.4.1. Newtonian fluids

Newtonian fluids have a linear relation between the applied shear stress, τ and the shear rate, dv/dy. In Newtonian fluids, the viscosity is only temperature and pressure dependent. A common term for Newtonian fluids is that they have a simple molecular formula and a low molecular weight (RheoSense, Web-2016). An example of a Newtonian fluid is water, which is going to be used as the only fluid in this thesis.

2.4.2. Non-Newtonian fluids

A non-Newtonian fluid is a fluid that exhibits a non-linear relation between the applied shear stress, τ and shear rate, dv/dy. In non-Newtonian fluids, the viscosity, in addition to temperature and pressure, is shear stress and shear rate dependent (RheoSense, Web-2016).

There are mainly three types of non-Newtonian fluids. Figure 2.1 shows the comparison of a Newtonian fluid relative to the types of non-Newtonian fluids, where the x-axis stands for shear stress and the y-axis for shear rate.

- Pseudoplastic: Shear-thinning fluids, which means that the viscosity decreases as the shear rate increases. The transition between plastic and pseudoplastic can be hard to distinguish.
- Dilatant: Shear-thickening fluids, which means the viscosity increases as the shear rate increases.
- Bingham plastic: Linear shear stress/rate ratio.

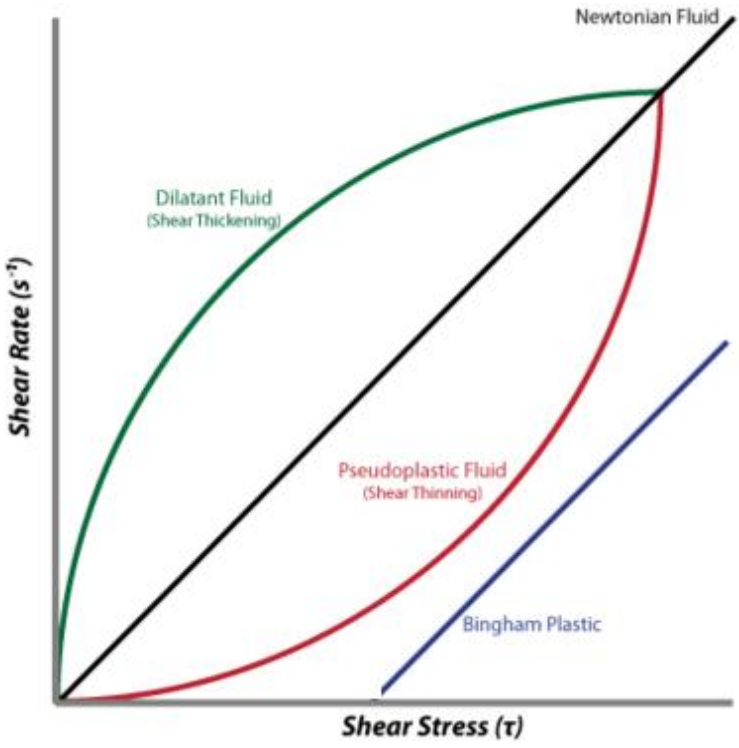

Figure 2.1: Comparison of Newtonian and non-Newtonian fluid

2.4.3. Slurry flow

In this thesis, slurry flow is defined as a two-phase flow that contains both liquid and particles. Many problems due to slurry flow can be simplified because one velocity component is dominant. Pipe flow certainly falls into this category and an equation for a finite control volume can be considered (Shook & Roco, 1991).

The mean velocity U_m for a multiphase mixture is defined as the volumetric flow rate divided by the area, $A = \pi D^2/4$. In terms of the flow rates Q_P and Q_L of particles and liquid.

$$U_m = \frac{Q_P + Q_L}{A} \tag{2.4}$$

2.4.4. Turbulent flow

Turbulence is a phenomenon of fluid flow that occurs when the momentum effect dominates viscous effects high Re. This type of flow consumes a lot more energy than simple gliding of fluid layers in laminar flow, this is due to its irregular, random and chaotic movements. Turbulence flow is characterized by random fluctuating motions of the fluid masses in three dimensions and is characterized by randomly fluctuating velocity fields. The fluctuating velocity fields manifest themselves as eddies or regions of swirling motion. The kinetic energy in the small eddies are transformed into internal energy, which means that the turbulent flow is dissipative. The small eddies receives the kinetic energy from slightly larger eddies while the largest eddies extract their energy from the mean flow. (Menge, 2015)

2.5. Flow patterns

Slurry (liquid-particles) flow is very complex and the definition of the flow patterns in slurry flow relies mainly on visualization. This is the main reason why various reports assign different characteristic for the flow patterns. Turian and Yuan (1977) divided the patterns into four categories, where they used the term “saltation” for what Pinchas Doron and Barnea (1995) referred to as “moving bed”. The amount of flow patterns categories depends on the grade of precision the report authors chooses. Lazarus and Neilson (1978) had a very precise division of patterns, with a new name for every change in the settling of particles. Brown (1991), on the other hand, had only two categories depending on whether the flow was “heterogeneous” or “fully-segregated”. The “heterogeneous” flow included both flows with moving beds and with

a heterogeneous suspension out from the definitions made by Pinchas Doron and Barnea (1995), “fully segregated” was equal to Doron and Barneas definition on homogeneous flow. The definitions of the transition flow rates between the patterns varies often because of these two reason, visualization and number of patterns.

2.5.1. Doron & Bernea’s definition of flow pattern

One of the deviations of flow pattern that is often used is Pinchas Doron and Barnea (1995) which takes a lot of experience from earlier studies into account and groups together flow patterns with similar behavior. The definition of flow pattern they came up with is as follows:

(1) **Fully suspended flow**, All the solid particles are suspended. The fully suspended flow pattern may be subdivided into two sub-patterns:

(a) *pseudohomo- geneous suspension*, when the solids are distributed nearly uniformly across the pipe cross-section. The mixture velocities required for such flow are usually very high and cannot be considered practical.

(b) *heterogeneous suspension flow*, when there is a concentration gradient in the direction perpendicular to the pipe axis, with more particles transported at the lower part of the pipe cross-section. This is the case in most practical applications.

(2) **Flow with a Moving Bed (MB)**, solid particles accumulate at the bottom of the pipe. Thus they form a packed bed layer, which moves along the pipe bottom. The concentration of this layer corresponds to maximal packing, or nearly so. A heterogeneous mixture occupies the upper part of the pipe cross-section.

(3) **Flow with a Stationary Bed (SB)**, a stationary deposit is observed at the bottom of the pipe. On top of this deposit particles are transported as a separate moving layer. In many cases one observes dune-like forms on the upper part of the bed, a phenomenon known as "saltation". The rest of the pipe is still occupied by a heterogeneous mixture, though its concentration profile is much steeper than in the other flow patterns.

2.6. Visualization and image analysis

Visualization of particle motion is an important source of information about different flows. Information about the flow can be used to describe the flow pattern, explain pressure drop and show velocity profiles to mention some of its utility. The capabilities of the flow visualization techniques have been well developed over the years. It is now possible to measure point velocity simultaneously in a flow field, to track an assembly of particles in a controlled volume and to determine local concentration of particles (Shook & Roco, 1991). There are many different ways to measure particle velocity. This thesis, is going to look closer into PIV and UVP measurement techniques.

2.6.1. Particle image velocimetry

The PIV method is an optical method of flow visualization used in education and research. The method was taken into use because it was difficult to know the fluid motion in a homogenous fluid. PIV is non-intrusive and measures the velocities of micron-sized seeding particles following the flow in both two and three dimensions. The PIV method applied in this thesis is called time resolved PIV and uses a high-speed camera at a fixed frame (Keane & Adrian, 1992).

When using the PIV method, small seeding particles are added into the flow. These particles are small and light enough to not affect the flow dynamics. A strong laser illuminates the flow in order to make the seeding particles work as scattering sites for the light, which makes them visible in the images taken by a high-speed camera at a fixed frame. The illuminated particles makes it possible to detect the flow velocity of the fluid by processing the images. The high-speed camera is connected to the Pylon viewer program, which controls the settings on the camera. As figure 2.2 shows, the images of the flow are divided into small subsections called interrogation areas. The interrogation areas for each of the image frames are cross-correlated with each other to derive the most probable particle displacement in the interrogation areas. The cross-correlation gives a peak that indicates the common particle displacement, $\Delta\bar{x}$. Sub-pixel interpolation is applied to achieve an accurate measurement of the displacement. When the cross-correlation analysis is completed on all frames, a velocity vector map over the whole target area is obtained, by using the equation 2.5. The time interval, Δt between each image is

constant due to a shutter in the camera. The time is taken into account to give a vector velocity, $\bar{v}$ for the particle (Keane & Adrian, 1992):

$$\bar{v} = \frac{\Delta \bar{x}}{\Delta t} \tag{2.5}$$

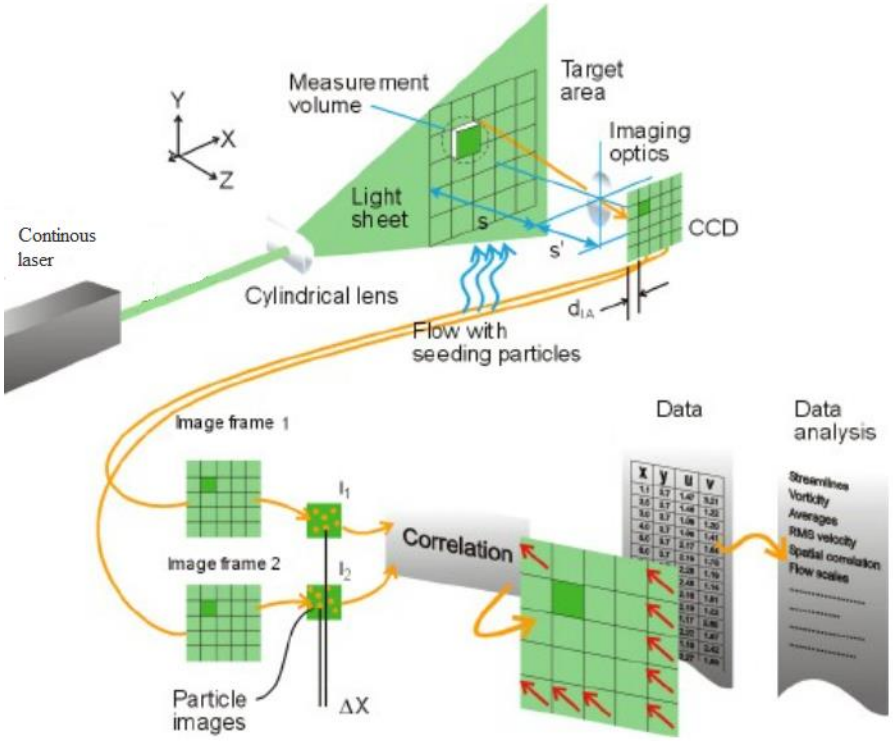

Figure 2.2: How PIV finds the particles displacement in the target area

2.6.2. Ultrasonic velocity profiling

A UVP monitoring instrument is used for measurement of shear, turbulence and friction for particles transport and bed dunes dynamics in circular pipes. The working principle of the UVP method is based on using a pulsed ultrasonic Doppler effect together with an echography relations. A. Rabenjafimanantsoa, Time, and Saasen (2007) showed that UVP measurements are very useful measurements on liquid-particle flow. UVP have an advantage in opaque systems where PIV can not be used. Since UVP is a one-dimensional technique, proper care must be shown to draw valid conclusions in three-dimensional flows (A. Rabenjafimanantsoa et al., 2007).

The measurement principle for UVP is that the transducer transmits a short emission of ultrasound that travels along the measurement axis, and then the transducer switches over to receiving. When the ultrasound pulses hit the small seeding particles in the liquid, part of the ultrasound energy scatters on the particle and echoes back. After a time delay, the echo reaches the transducer. If the seeding particles are moving (velocity > 0 m/s) into the acoustic axis of the transducer, Doppler shift of echoed frequency takes place, and received signal frequency becomes "doppler-shifted". By using the time delay and Doppler shift frequency, it is possible to calculate the position and velocity for each of the particles on the measuring axis. Information about the position is given by the time used from sending out the pulse until it is received again, multiplied with the sound velocity in water. While the velocity information is derived from the instantaneous Doppler shift frequency at that instant. The time it takes from the transducer emits a pulse sound wave until it reaches the maximum depth and returns back to the transducer, is called sampling period. In order to develop a velocity profile, the procedure of emitting and receiving is repeated many times (Guney, Bombar, Aksoy, & Dogan, 2013). The velocity profile is formed by processing the echo signal in such a way that the instantaneous frequency is estimated at each instant. The system used to realize this kind of signal processing, requires intricate analogue and digital electronics. (Takeda, 1999)

The UVP measures the velocity, v_{UVP} and distance, d_{UVP} on the measurement axis. The velocity in horizontal direction, $u_{Horizontal}$ can be calculated by using eq. 2.6. The angle of the transducer, θ_{trans} and u_{UVP} is needed (Guney et al., 2013). To be able to plot the velocity in horizontal direction, the distance at horizontal, $u_{Horizontal}$ needs to be calculated, by using eq. 2.7.

$$u_{Horizontal} = \frac{u_{UVP}}{Sin\theta_{trans}} \tag{2.6}$$

$$d_{Horizontal} = d_{UVP} * Cos\theta_{trans} \tag{2.7}$$

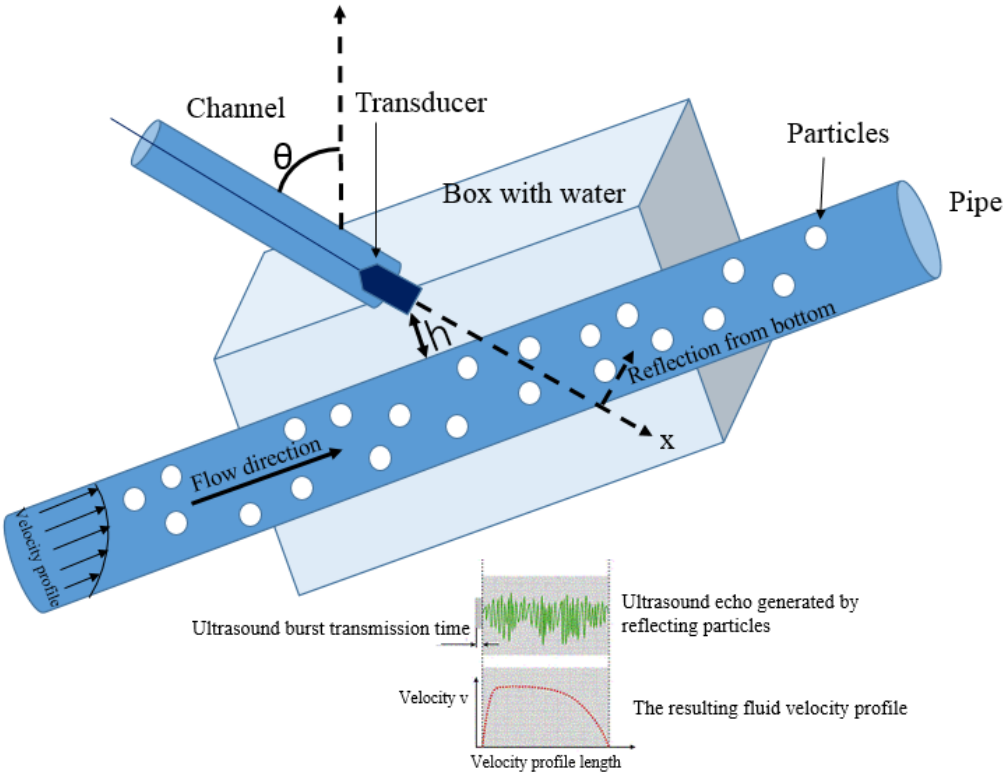

Figure 2.3: The UVP setup and the measured values showing on the computer

Figure 2.3 shows the UVP setup and what the results measured by the transducer looks like. The dotted line indicates the x-axis for the measurement. The box around the pipe is filled with water to get as little background noise as possible.

2.6.3. Uncertainty assessment of image post processing

The main issue in the post processing is to find a way to check the uncertainty and limitation in the MATLAB script that is applied to detect the particles. To find out how accurate the post processing is, several samples have to be taken into account.

The optical setup, particle slip and bad quality on the pictures can lead to errors in the measurement. PIV is based on algorithms and therefore there is an uncertainty due to whether the algorithms are accurate enough.

3. Experimental work

In this chapter a detailed description of the medium-scale flow loop, of the equipment used for different measurement techniques, of the flow properties and of the measurement methods applied is given. The flow loop used in this thesis is already built and used for earlier studies. In this thesis, the flow loop was used to run different experiments with turbulence flow in single-phase water flow and two-phase liquid-particle flow. Experiments on two-phase flow was run both with and without a rotating DS, to get a better understanding of the complex flow details. To be able to get a good view of the velocity profile in the pipe, two different measurement techniques, PIV and UVP, were applied.

3.1. Experimental setup

The medium-scale flow loop was built up with fully transparent glass pipes that had an ID of 40 mm and a wall thickness of 2,3 mm, the length of the flow-loop was approximately 14 m. A simplified sketch of the flow loop is shown in figure 3.1, the numbers (1-13) indicates different equipment and are named on the left side in the figure. The sketch shows all the different test sections, equipment setups used for PIV, UVP and particle mass flow rate as well as where the pressure taps are placed.

In order to keep the pressure and amount of particles in the loop constant, the flow loop was a closed-circuit loop. The flow loop system contained four different test sections, one horizontal, one bend section and two inclined sections (5^0 and 35^0). In each of the sections, two pressure taps were connected together to a pressure transducer to measure the DP, one at the low-pressure side and the other one at the high-pressure side. All of the pressure transducers were connected to a program called LabVIEW. This program shows all of the measured DP values.

The pressure created by a screw pump pressured the fluid flow around in the flow loop. To avoid variations caused by the pump, a pressure column was used to keep the pressure constant. The effect of the pump was determined by the set frequency on the frequency converter, which also controlled the mass flow rate. A Coriolis flowmeter was used to measure directly the true mass flow rate of the fluid traveling past a fixed point per unit time. The Coriolis flowmeter was connected on the pipe and sent the calculated flow rate and density to the LabVIEW

program. Before entering the test sections, the flow went through a Venturi mixer, where the particles were re-injected when there was a two-phase flow. After the last test section (35^0 inclination), the flow entered a hydro cyclone, which separated the particles from the liquid, when the flow was two-phased. The first time particles were added in to the flow, it was by opening the hydro cyclone. The liquids in the hydro cyclone went back to the tank and when the flow was two-phased, the particles fell down into a column connected to the Venturi mixer. To be sure that no particles entered the tank, a homemade "separator" was made out from an plastic container. The "separator" was placed in front of the outlet, inside the tank. In two-phase flow it was possible to decide if a particle re-injection was wanted or not, due to a valve connected to the column. All the data, mass flowrate, density, velocity and the four different DP measured in the loop were shown in the LabVIEW program, which made it possible to save the data and use it for further processing.

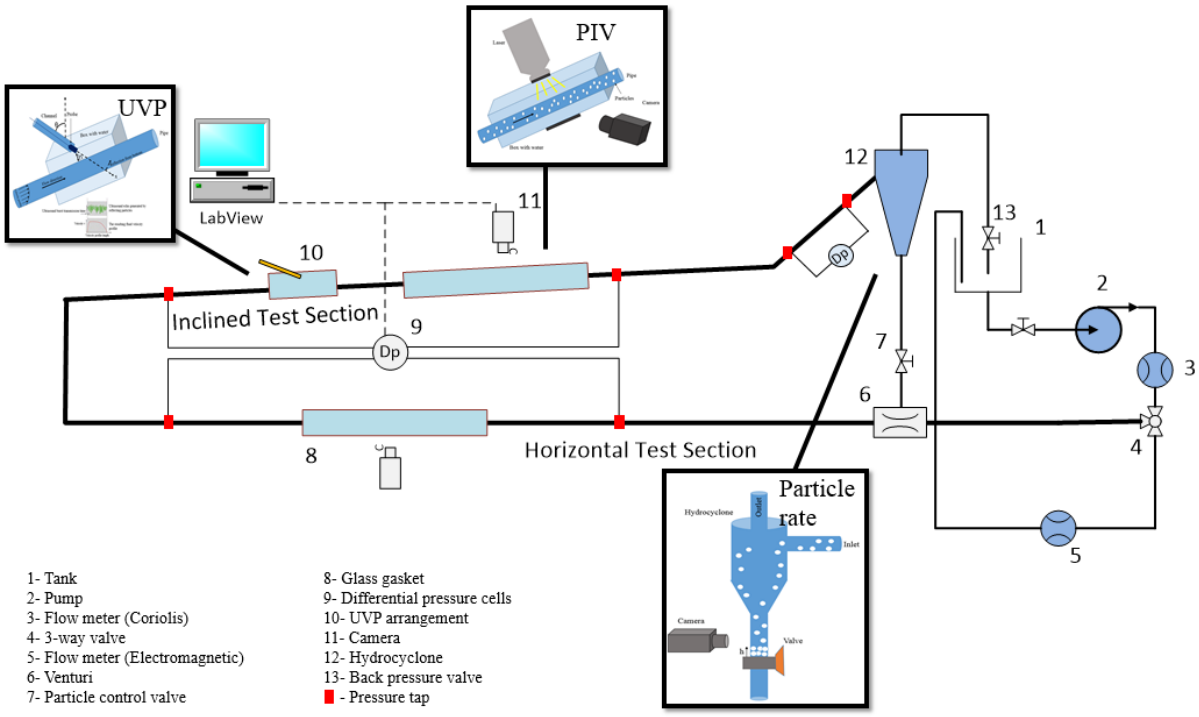

Figure 3.1: Medium flow-loop with the experimental setups

3.1.1. Differential pressure

Rosemount delivered the four pressure transducers, Model 3051 Smart Pressure Transducer. The pressure transducers measured in the range from $-62\ to\ 62\ mbar$.

3.1.2. Rotating drill string

To run the experiments simulating the effect of a rotating DS in an inclined wellbore, a DS was made and pushed into the pipe in the 5^0-inclined test section. The DS was made by connecting three plastic pipes with an Outer Diameter (OD) of $25\ mm$, with two flexible joints, the total length of the DS in total was $4{,}60\ m$. In the sections with the joints, the OD of the pipe increased to $31\ mm$, the length of the joints were $0{,}1\ m$. The DS was filled with water containing potassium permanganate, which gave the water a pink color. The DS was blocked in both ends by a rubber plug. A smaller pipe with a large plug around and a locking mechanism were pushed into one of the rubbers, to connect the DS to the motor. The large plug was used for blocking the main flow loop pipe. The motor system rotating the DS consisted of a motor (DCX 22 L), a gearhead (GPX 22 C, 2-stage) and an encoder (ENX 16 EASY), all the parts were delivered by Maxon Motors. The motor was connected to an encoder, which was controlled by a program called Escon. Escon controlled the settings on the motor and made it possible to decide the rpm on the DS and to record the actual rpm delivered to the gearhead when running. To make it possible to see the rotation on the DS two black ribbons with equal distance between each other were glued on the surface of 1/3 of the "drill string". Figure 3.2 shows a drawing of the 5^0 -inclined test section with a DS. The drawing shows a sketch of what the drill string looks like, the equipment used to make it rotate and the lengths between pressure taps, joints and joint-pressure taps.

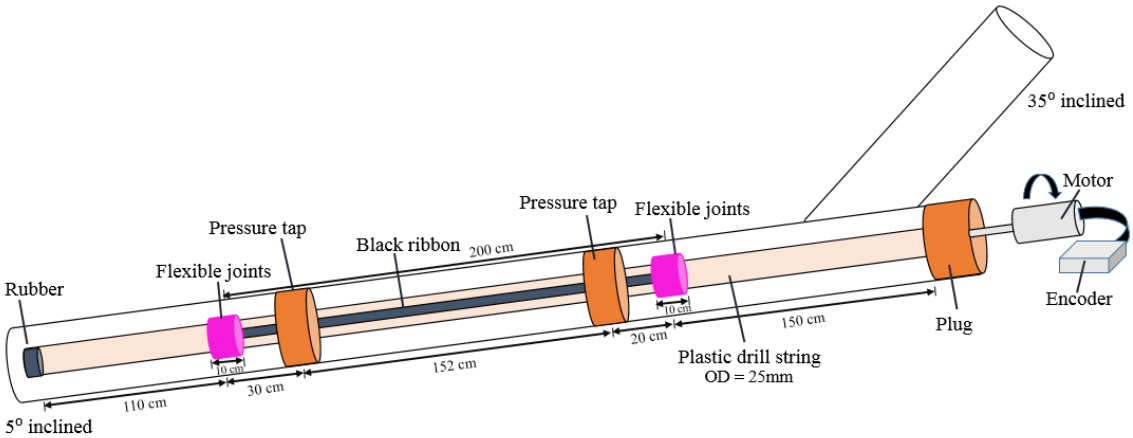

Figure 3.2: Drawing of the 5^0-inclined test section with a homemade DS

3.1.3. Particles mass flow rate

The equipment used to measure the particles mass flow rate was set up in front and in the back of the column under the hydro cyclone. The column was transparent and had an ID of $40\ mm$, a valve in the end of the column controlled the re-injection of particles. A board ($120x30\ cm$) with white Light Emitting Diode (LED) light containing $49\ LED\ x\ 1W$, was mounted behind the column. A Basler camera (acA800-510uc) connected to Pylon Viewer was mounted on a tripod in front of the column. The Basler camera recorded up to $511\ fps$ in full resolution $600x800\ pixels$. In this thesis the camera was set to $500\ fps$. The Pylon Viewer program controlled the settings and saved the images on the computer. Image viewer, an app in MATLAB, was used to process the images.

3.1.4. Particle image velocimetry

All the equipment needed for using the PIV measurement technique was installed in the test sections with 0^0 (horizontal), 5^0, and 35^0 inclination. Seeding particles (38A2111) with an average diameter of $20\ \mu m$ were added into the tank. A high-speed video camera (SpeedCam MiniVis e2) was set on a tripod in front of the pipe, utilized to record the particle movement. The camera recorded up to $2500\ fps$ in full resolution $512x512\ pixels$, and for this thesis the frame rate was set to $2000\ Hz$. Above the pipe, a $532\ nm$ green laser (Photon DPGL-2200) was mounted to illuminate along the center of the test section. The laser was only used in some parts of the experiment. Two of the same board used for finding the particles mass flow rate were mounted. Figure 3.3 shows a picture of the PIV setup without the green laser. The picture shows how the white LED light in back and front lightens up the test section and the quality of an image taken by the high-speed video camera. The image taken by the high-speed camera shows particles moving along the DS inside the pipe, the black lines are ribbons on the surface of the DS. The PIVlab app available in MATLAB, was used to process the images taken by the high-speed video camera.

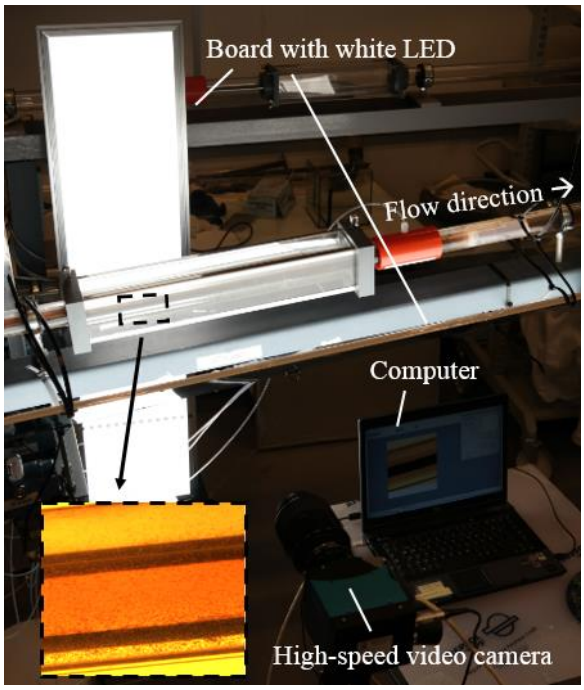

Figure 3.3: Picture of PIV measuring setup and an image of the flow, taken with the high-speed video camera

3.1.5. Ultrasonic velocity profile

In the test section with 5^0 inclination the equipment used for measuring UVP was set up, Figure 3.4 shows a simplified picture. Seeding particles (AX-SEED82) with a diameter range of $80 - 200\ \mu m$ were added into the tank. A rectangular $(15x10x10\ cm)$ glass box was mounted around the pipe. On the top of the box, a cylinder with a drilled channel in the middle, was mounted. A rectangular area under the cylinder was cut out from the top of the box, to make it possible to move the cylinder in the angle that was wanted. A transducer was pushed down in the channel and as close to the pipe as wanted. The transducer was connected to the UVP DOU delivered by MET-FLOW AS. With the use of different transducers, the UVP DUO can produce five emitting frequencies. In this thesis the transducer (TX-4-5-8-40) was used, it had an active part with an OD of $5\ mm$ that sent out emitting frequencies of $4\ MHz$. The transducer had a measuring distance range of $0{,}003 - 3\ m$ and could measure velocities in the range of $0{,}0456 - 46{,}25\ m/s$. The UVP DUO was connected to a computer, where the settings were controlled and the results saved by UVP for Optek firmware, program delivered by the supplier.

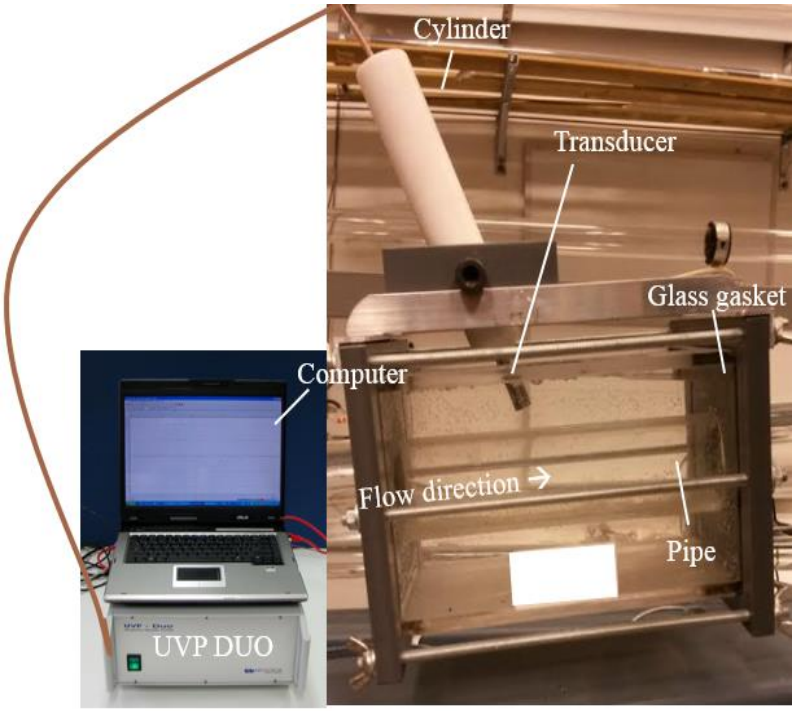

Figure 3.4: UVP measuring setup

3.2. Fluid and particles properties

In the thesis, pure water was used to run single-phase water flow and pure water consisting glass particles were used to run two-phase liquid-particle flow. The glass particles added to the flow, served one main purpose, creation of sedimentary beds. In this thesis two different concentrations of particles were used, 8,5 % for the experiments without drill string and 12,5% for the experiment with DS. The concentration was increased to make it easier to see the effect of the DS. The diameter of the glass particles were in the range between $240 - 320\mu m$ and were used in the two-phase liquid-particle flow. To find the average diameter and shape of the glass particles, an image of the particles was taken with a Scanning Electron Microscope (SEM). SEM is an electron microscope with a focused beam of high-energy electrons to generate different signals of solid samples through a scan. The produced signals contains information about the topography (texture) of the samples surface. Figure 3.5 shows the image taken by the SEM, the image shows the shape of the glass particles. Figure 3.6 shows a plot of the distribution, the particles diameter is along the x-axis, and the y-axis shows the amount of particles with given diameter. The distribution was found by processing the image taken by the SEM in Image viewer. The average diameter of the particles was found to be $280\ \mu m$ and the shape was spherically.

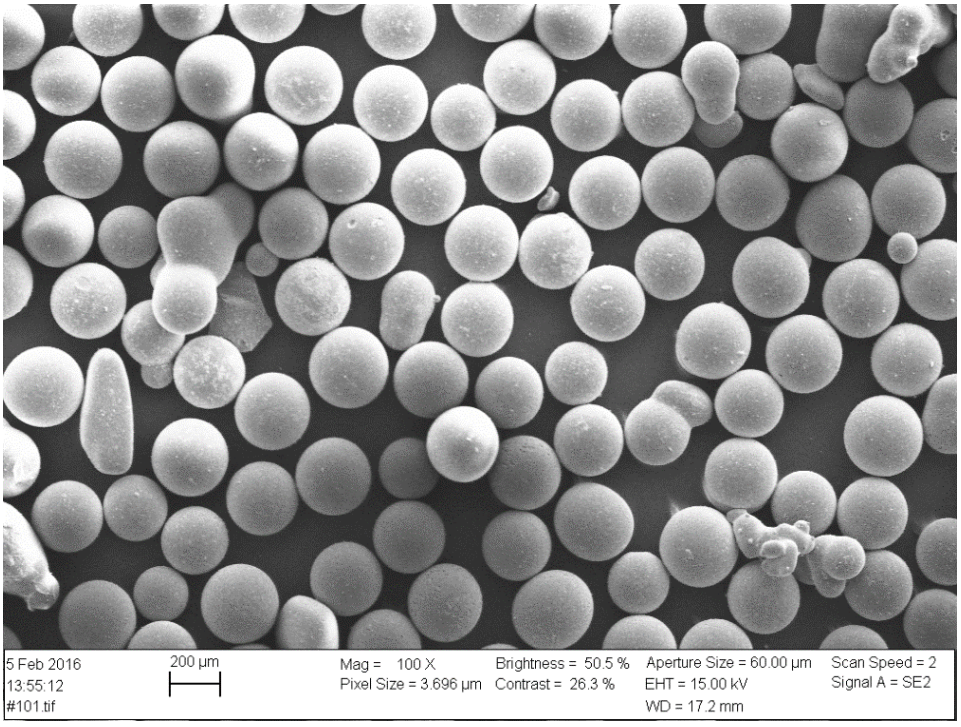

Figure 3.5: SEM picture of the particles

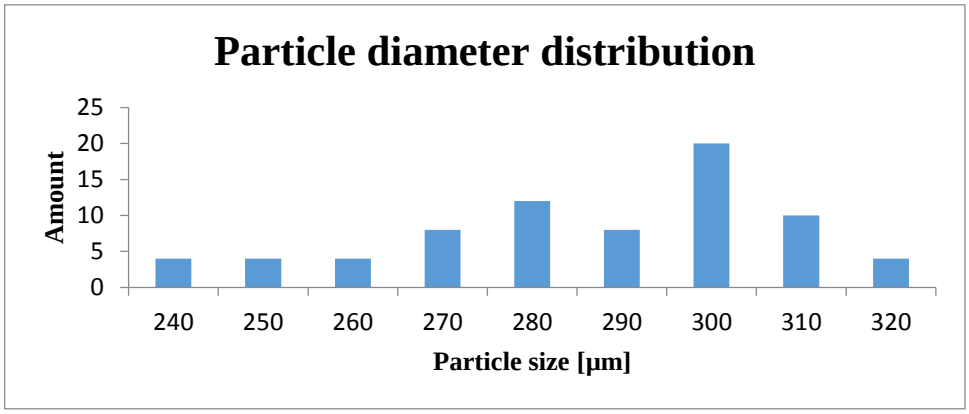

Figure 3.6: Plot of the distribution of the different particle size

The seeding particles (AX-SEED) used for UVP had a diameter range of $80 - 200\ \mu m$. The seeding particles were added to make the flow visualization possible and to act as ultrasonic reflectors. The supplier MET-FLOW AS suggested that the particle diameter should be at least a quarter of the ultrasonic wavelength, λ or higher.

$$d_{sp} \geq \frac{\lambda}{4} \tag{3.1}$$

Where d_{sp} is the particle diameter and,

$$\lambda = \frac{c}{f} \tag{3.2}$$

The speed of sound in water, $c = 1500\ m/s$ and f is the frequency that was 4 MHz in this thesis. This gives a requirement around 94 μm (H. Rabenjafimanantsoa, 2007).

When the seeding particles (AX-SEED) had been into the loop for a while, they started to stick together and float up to the surface of the water tank. Smaller seeding particles (38A2111 PSP20) delivered by Dantec were chosen to use for PIV, these had an average diameter of 20 μm.

Tabell 3.1: Fluid and particle properties

	Density $[kg/m^3]$	**Material**
Fluid, water	1000	Water
Glass particles	2650	Glass
Seeding particles (AX SEED)	1070	Copolyamid
Seeding particles (38A2111 PSP20)	1030	Polyamid

3.3. Methods

In this sub-chapter, all of the different methods to get a better understanding of the complex flow details applied in this thesis, are described. In this sub-chapter, all of the different methods applied in this thesis to get a better understanding of the complex flow details, are described. The methods describes how the experiments are conducted to see how pipe inclination, flow rate, DP, velocity profile and rotation on DS affects the particle transport.

3.3.1. Rotating drill string

Since the motor was new, experiment on the actual rpm on the DS had to be performed. The experiment was done by counting the amount of rotations on the DS in one minute at different flow rates. The result showed that the insert value in the settings had to be 25 times higher, than the wanted rpm.

For all the experiments with a rotating DS, the rotation speed was set to $0,\ 20,\ 35,\ 70$ and $100\ rpm$. The superficial velocity of liquid (Usl) in the 5^0-inclined test section, $Usl_{annulus}$ was calculated out from the measured Usl in the flow loop. The change in Usl for the 5^0-inclined test section was due to change in size of area when the drill string was added. ID_{pipe} stands for the Inner Diameter of the pipe and OD_{DS} for the outer diameter of the drill string.

$$Usl_{annulus} = \frac{Usl * {ID_{pipe}}^2}{(ID_{pipe} - OD_{DS})^2} \tag{3.3}$$

In order to see the effect of the DS as good as possible, the concentration of particles was increased from 8,5% to 12,5% by adding more particles into the flow loop. To be able to keep the particle concentration at 12,5%, the experiments with DS could only be run for flow rates lower than $1{,}0\ m/s$.

3.3.2. Differential pressure

Before running the experiments, the pressure transducers were calibrated and the range of measuring was chosen depending on the estimated value of the DP for each of the test sections. When the DS was added into the 5^0 inclined test section, the range on the pressure transducer in 5^0-inclination was changed into a higher max value due to increase in the pressure. Table 3.2, shows the range for each of the pressure transducers and the distance between the pressure taps in each of the test sections. The tubes connecting the pressure taps to the pressure transducers were filled with water to get as little fluctuation in the measurements as possible.

Tabell 3.2: Distance between pressure taps and pressure transducer range

Pressure transducer	**Test section**	**Length [m]**	**Min value**	**Max value**
DP 0	0^0, Horizontal	1,52	-10	+10
DP 1	35^0 inclination	0,60	-10	+10
DP 2	5^0 inclination	1,52	-10/-40 (DS)	+10/+40 (DS)
DP	Bend	0,57	-10	+10

The DP at different flow rates was measured for both one- and two-phase flow with and without a rotating DS. The measured value for DP showed in LabVIEW for the different test sections, were calculated out from the measured pressures. P_H was the value measured at the high-pressure side and P_L was the value measured at the low-pressure side. Differential pressure, ΔP ig given by:

$$\Delta P = P_H - P_L \tag{3.4}$$

The measurements of the DP were done for single-phase flow and two-phase flow with and without a rotating DS. The DP was measured from high flow rate, 1,5 m/s (frequency 20) to low flow rate, 0,30 m/s (frequency 4). When the pressure transducers showed stable measurements of the DP, the data were recorded in LabVIEW over a period of time that always lasted for more than 5 minutes. The recorded data were then saved and processed in MATLAB, were the measured values from the pressure transducers, were divided by the length between the pressure taps. The MATLAB script used a moving average filter on all of the different

measured data. MATLAB calculated the average value for all of the measured data at a specific frequency. The results on DP for single-phase flow without DS was plotted together with the calculated DP using Haaland correlation. The Darcy friction factor was calculated with Haaland correlation, eq. 2.1 and with the use of the factors given in table 3.3. The calculated DP, ΔP was found by,

$$\Delta P = f_f \frac{dl}{D} \rho \frac{Usl^2}{2} \tag{3.5}$$

Where f_f stands for Darcy friction factor, dl for length of the test section, D for diameter, ρ for density of fluid, Usl for superficial velocity of fluid.

Tabell 3.3: Factors needed for Haaland correlation

	Values
ε - Roughness	$5*10^{-5}$
D - Diameter [mm]	40
A - Area [m^2]	$1{,}3*10^{-3}$
μ - Dynamic Viscosity [Pa*s]	$1{,}002 * 10^{-3}$

The result for single-phase flow with DS and two-phase flow with and without DS were plotted into three different plots representing each of the three different cases.

3.3.3. Particle mass flux rate

For different frequencies, a series of images of the column above the particle re-injection were taken, while the column was filled with particles (valve closed). Two and two images with a large distance between them were opened in Image view. In image view the pixel number in the y-direction at the surface of the dark particle area was found for h_1 and h_2. Figure 3.7 shows what the images looked like, and how the height, h was defined. The purpose was to detect the increased height of particles in the column from the beginning to the end by calculating the Δh. A scale was made to convert pixels to mm. The time intervall between the two images was known based on image numbers and settings on the camera. The Δh was used to calculate the volume of particles in a time intervall. It was then possible to calculate the superficial velocity of particles (Usp) at different flow rates. The changes in Usp due to different flow rates were looked into.

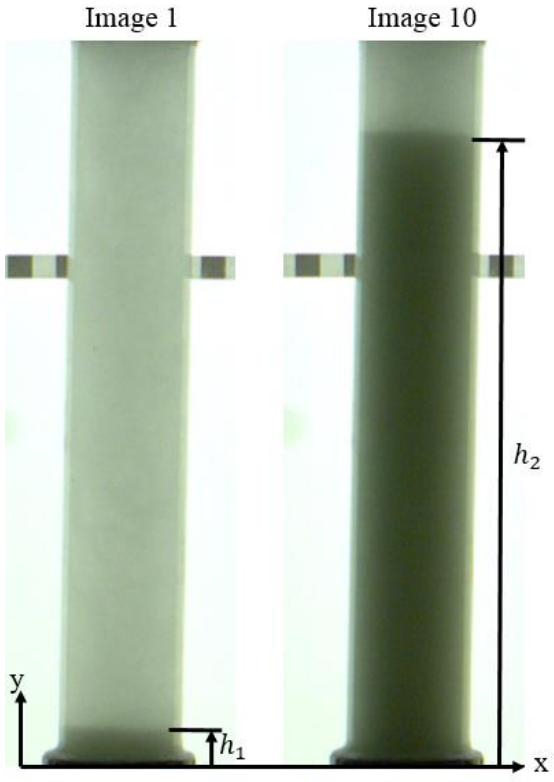

Figure 3.7: Images of two columns used to detect the increased column height over a period of time

3.3.4. Detection of flow pattern

A definition of the flow patterns were made based on observations and literature review. Written definitions were put together with drawn illustration. The two-phase flow was observed visually through the transparent pipes at different flow rates and notes were made. Plots were made to show the different flow patterns for different velocities in each of the test sections.

3.3.5. Particle image velocimetry

Section 2.6.1 gave a good description on how the the PIV measurement technique works. In this thesis, the PIV measurement technique was used on single-phase flow and two-phase flow with and without a rotating drill string to look at the velocity profile in one direction. The camera was adjusted to take a series of images at a known speed, at different flow rates for all the three cases. From the stack of image series, an amount of 100 images was taken out and changed to black/white images by using a MATLAB script. The images were then imported into PIVlab1.4.

PIV in PIVlab consists of three main steps, pre-processing, image evaluation and post-processing. In the pre-processing, different selections are done based on the area that is of interest, how fast the particles move and which filter detects most particles. When the analysis is run, a vector validation and calibration is applied based on the known distance in picture and settings on the camera. Figure 3.8, illustrates the different settings that are possible to apply at different stages, as well as what type of post processing that is possible to use in PIVlab.

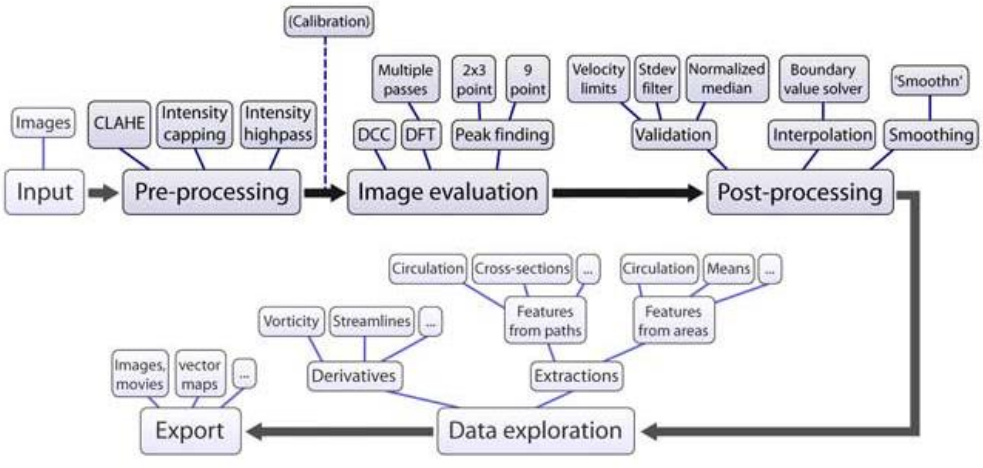

Figure 3.8: Illustration of the different possibilities when using PIV analyses in PIVlab (Thielicke & Stamhuis, 2014)

Pre-processing were used in all cases, to get as many visible particles as possible. An Fast Fourier Transform (FFT) window deformation algorithm, three different passes ($64, 32$ and $16\ pixels$), interpolator spline and Gauss2x3-point as sub-pixel estimator were chosen. The velocity limits were selected based on were most of the points appeared. The pipe diameter was used as the calibration distance and the time between the pictures as time interval. Before calculating a mean vector, the data were smoothened. A poly-line was drawn in the images, the amount of interpolated points was set to 300, before the u and v component were extracted and the values for the whole series of images were saved as a ASCII chart. The ASCII charts were then opened in Excel and plotted to see the tendencies of the velocity profiles at a given flow rates. For the inclined sections, the u and v components and distance, d_{PIV} measured had to be recalculated in order place the x-axis in the flow direction and distance direction 90^0 from flow direction. The u component in flow direction was then named u_θ and the v component in the direction 90^0 from flow direction was named, v_θ. The new calculated distance had the same direction as the v component and was named d_θ. The θ stands for degrees of inclinations and it changes depending on which test section that was used. To do the recalculation, equation 3.6, 3.7 and 3.8 were applied, together with the u and v component saved in the ASCII.

$$u_\theta = ucos\theta - vsin\theta \tag{3.6}$$

$$v_\theta = usin\theta + vcos\theta \tag{3.7}$$

$$d_\theta = Cos\theta * d_{PIV} \tag{3.8}$$

The velocity profiles measured with PIV for different flow rates were then compared to each other.

3.3.6. Ultrasonic velocity profile

Section 2.6.2 gave a good description of how the UVP measurement technique works. In this thesis the UVP measurement technique was only applied for single-phase flow in the 5^0-inclined test section. A transducer was pushed through the channel in the cylinder and placed as close to the pipe as possible with an angle = 20^0 during the entire experiment. The data was saved and opened in Excel to calculate the velocity in horizontal direction out from the velocity measured by the UVP. The velocity in horizontal direction was recalculated by applying eq. 2.6. To be able to plot the measured velocity profile, the distance had to be recalculated to vertical, by applying eq. 2.7. The velocity profiles measured with UVP for different flow rates were than compared to each other and with the results from PIV.

3.3.7. Bed height

In the two-phase flow, it was possible to see the bed height of the particles. The images taken for PIV analyses in horizontal and 5^0-inclined test sections, were now used to measure the bed height at different flow rates, with and without a rotating drill string. The images were opened in image view and the height of the bed was found by looking at the pixel number differences between the surface and bottom of the bed in y-direction. The height of the bed at different velocities was compared.

4. Result and discussion

In this chapter, all the results from DP measurements, particle mass flow rates, visual observations, PIV and UVP for the three of the different test sections will be presented. The changes in DP, flow pattern and velocity profile in single- and two-phase flow due to change in inclinations, flow rates and rotations speed of the DS will be investigated. Figures will be used to show plots of the measured data.

4.1. Differential pressure

The plotted DP measurements shows the average value of DP measured during a time interval. The experiments on DP are conducted to get an indication on how the pressure changes in single- and two-phase flow due to different flow rates, inclinations on the pipe and rotations speed on the DS. The result from the experiments will be presented in this sub-section. Due to problems with the pressure transducer in the horizontal test section, the pressure transducer in horizontal test section was switch out with the pressure transducer in the bend test section. It took time before a new pressure transducer was found and mounted, it is therefore only one DP measurements of the bend test section presented in this subsection. The velocity in the experiments varies between $0{,}5$ and $1{,}5\ m/s$ which leads to turbulent flow due to high Re.

4.1.1. Single-phase, water flow

A trend line for calculated DP with Haaland correlation is plotted together with the measured DP in each of the test sections. The roughness of the pipe, was set to $5 * 10^{-5}$. The horizontal test sections shows less measuring points, due to problem with the pressure transducer in the horizontal test section.

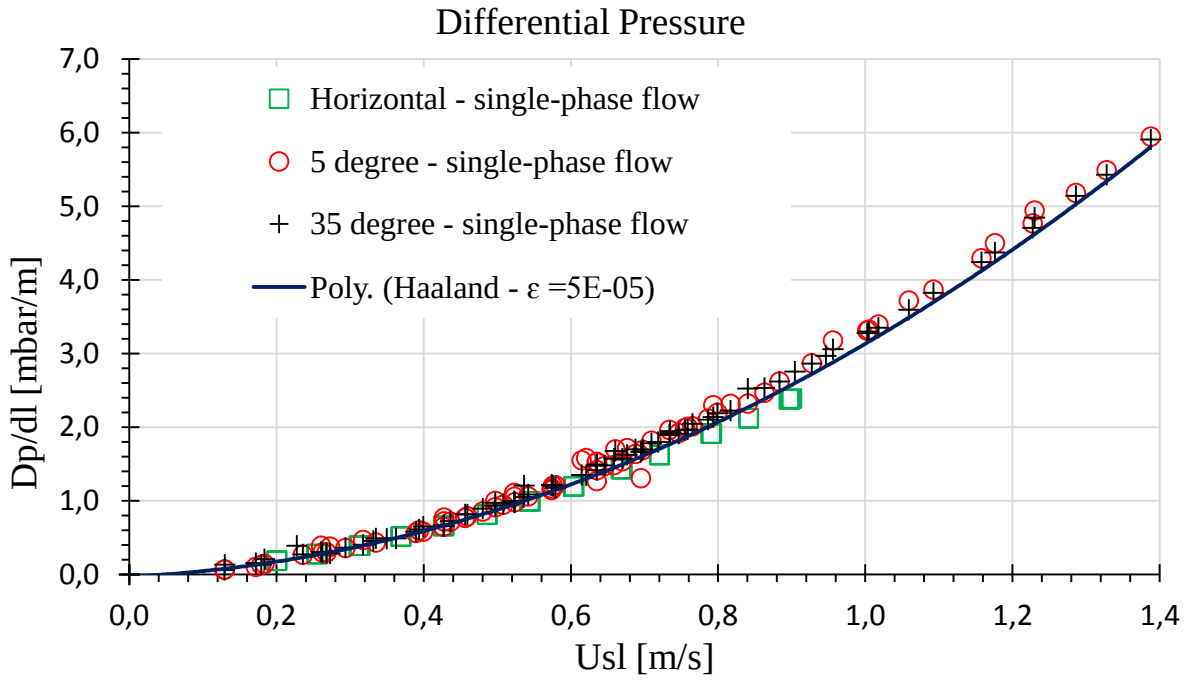

Figure 4.1: DP for each of the test sections together with the polyline for the calculated DP for single-phase flow

Figure 4.1 shows a plot of the measured DP in all the three test sections for single-phase flow together with a polyline of the calculated DP. The x-axis stands for the Usl and y-axis the DP over length of the test section. The plot shows that the measured pressure is almost equal to the calculated DP with Haaland correlation which increases with increased velocity. There are small differences between the measured DP in the three test sections, this indicates equal roughness on the pipe.

It is assumed that the kinetic pressure drop is so small that only hydro static and frictional pressure loss have to be taken into account when looking at the pressure drop. For the Horizontal test section, only the frictional pressure drop exist and it is therefore possible to conclude that frictional pressure drop increases with increased Usl. For the inclined test sections, the hydro

static pressure drop affects the total pressure drop in the pipe. The hydrostatic pressure drop increases with increased angle, which means that the 35°-inclined test sections has a larger hydrostatic pressure drop than the 5°-inclined test sections. Figure 4.1 shows an indication of higher pressure drop in the 5°-inclined test sections. This fact and observation indicates larger frictional pressure drop for the 5°-inclined test sections than for the 35°-inclined test sections, if kinetic pressure drop can be neglected.

4.1.2. Two-phase, liquid-particle flow

In two-phase flow without DS the overall particle concentration (C_p) was 8,5%. Due to the particles, more time was needed to get the flow properly stabilized. At low flow rates dunes occurred and a longer time of recording was needed (often up to 20 min) due to big variations in pressure caused by the dunes. To avoid loss of particles, the flow rate was kept under 1,3 m/s.

The measured DP in the three test sections are plotted together for comparison. For a better indication on how small the uncertainty in the measurements are, the standard deviation (SD) for each measurement is added into the plot. The polyline for the calculated DP in singe-phase flow is added, to show the increase in DP when it is two-phase flow.

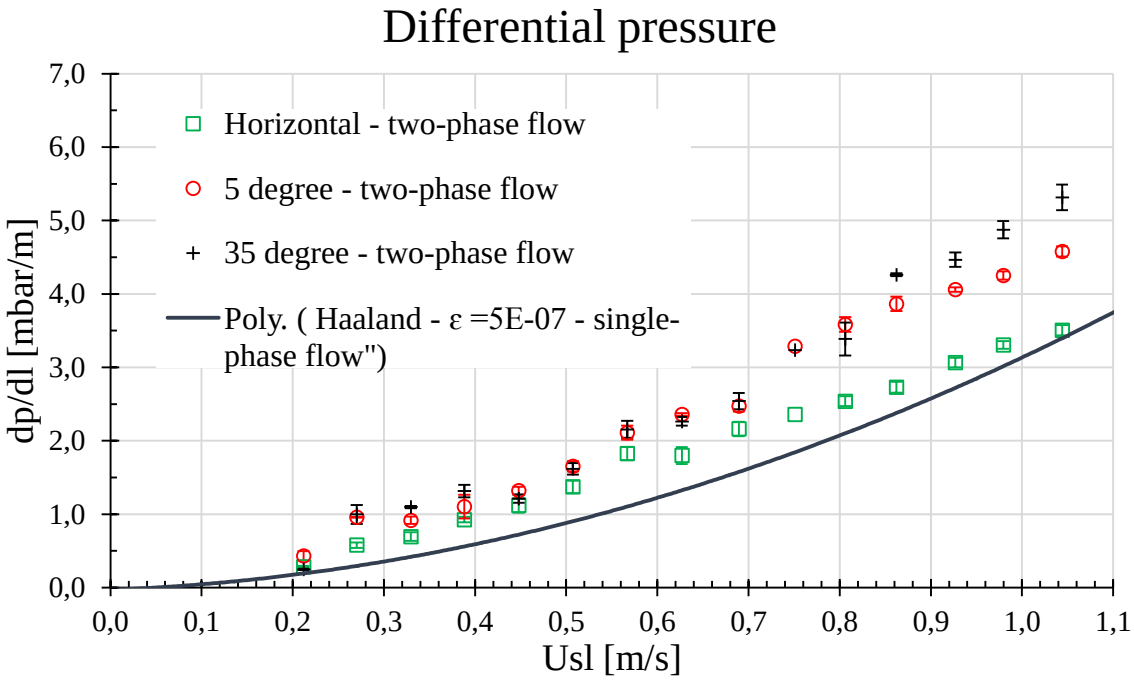

Figure 4.2: The measured DP with SD for each of the test sections in two-phase (C_p = 8,5%) together with the polyline of the calculated DP in single-phase flow

Figure 4.2 shows a plot of the measured DP and the calculated SD for all of the three test sections when it is two-phase flow. The polyline for the calculated DP in single-phase flow is assed into the plot. The x-axis stands for the Usl and y-axis the DP over the length of the test section. The plot in figure 4.2 shows that the pressure drop increases when it is two-phase flow and that an increase in inclination leads to larger pressure drop. The measured DP for the

horizontal test sections, shows a small bump in the measuring when the Usl is around 0,55 m/s. In the inclined test sections, the measured DP are close to equal, until the Usl reaches 0,85 m/s, then the 35°-inclined test sections shows a larger DP.

When particles are added into the flow, the flow area decreases and the pressure drop increases. Figure 4.2 shows a good indication of larger pressure drop in two-phase flow compared to the single-phase flow. The bump that occurs in the horizontal test section indicates a sudden change in frictional pressure drop. When the measured DP for the two inclined test sections differs from each other at high Usl it is due to change in frictional pressure drop.

4.1.3. Two-phase flow with a rotating drill string

When the DS was added inn to the 5^0-inclined test section, it was chosen to increase the overall C_p to 12,5%. Increased C_p made it easier to see the effect of different rotation speed on the DS. The increased C_p, increased the problem with keeping the particles in the flow loop, it was therefore decided to not run experiments with a higher flow rate than 1,0 m/s. During this experiment the pressure transducer in the bend section was working. A plot of each of the test sections were made to see how the DP are affected by changing rotation speed on the DS.

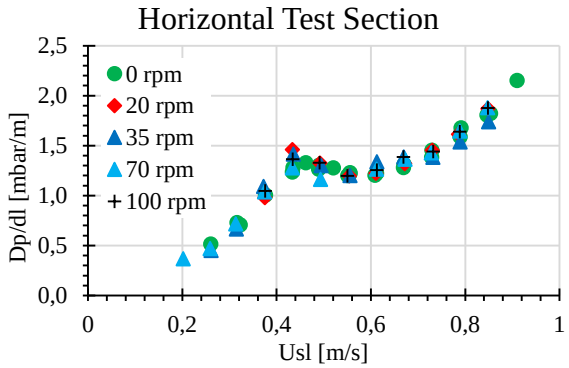

Figure 4.3: How the DP for different Usl are effected by different rpm in horizontal test section

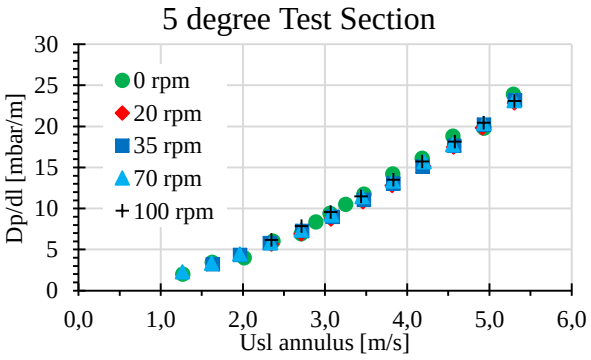

Figure 4.4: How the DP for different Usl annulus are effected by rpm in 5 ^{0}-inclined test section

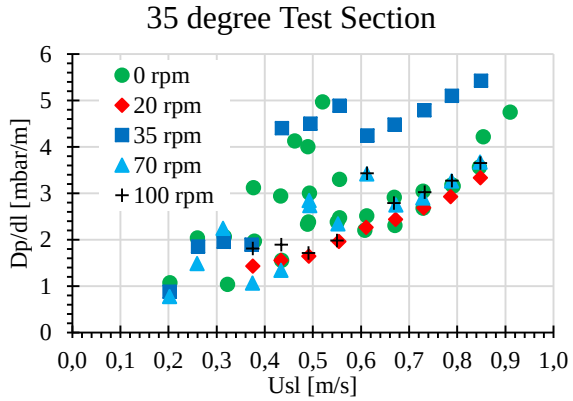

Figure 4.5: How the DP for different Usl are effected by rpm in 35 ^{0}-inclined test section

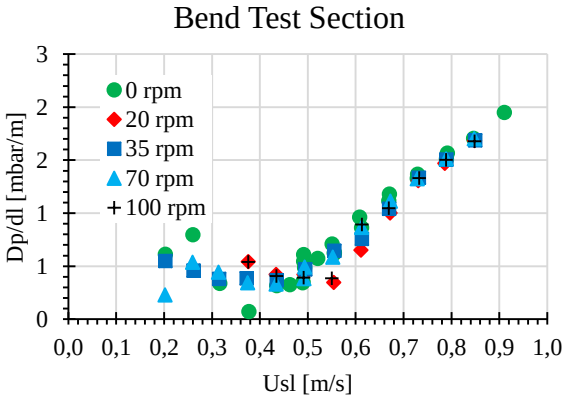

Figure 4.6: How the DP for different Usl are effected by rpm in bend test section

Figure 4.3, 4.4, 4.5 and 4.6 shows how the DP in the four test sections are affected by different rotation speed on the DS. The x-axis stands for the Usl (Usl in annulus for figure 4.4) and y-axis the DP overt length of the test section. Figure 4.3 and 4.4 shows no changes in DP due to change in rotation speed on the DS, the plots shows the same trends in measured DP as noticed in two-phase flow without DS. Figure 4.4 shows a linear trend of the measured DP. Figure 4.5 shows large differences in DP due to change in rotation speed on the DS, but no clear trend between rotation speed and DP is visible. Figure 4.6 shows differences in DP due to change in rotation speed at low velocities, but also here no clear trend is visible.

Figure 4.3 and 4.4 indicates that rotation on DS does not affect the DP in test sections where the DS is placed or in the test section before. It is important to take into account that the time series of raw data for DP had been averaged. If the raw data had been plotted, it would most likely have given another indication about the effect of a rotating DS. The bend section, figure 4.6 shows small change in DP due to rotation speed at low Usl. The changes might be due to collection of particles at the beginning of the DS that prevents smooth transport through the bend test section. The flexible joints on the DS caused a decrease in the annulus, affected the particle transport and causes problems with accurate DP measurements due to reduction in cross-section area. The plot shown in figure 4.4 did not fit in with the observation done by Duan et al. (2010) where they found that increased rpm leads to reduction in frictional pressure drop. The reason for this may be because of the average DP value, different particle characteristic, experimental setup or methods used to measure the DP. Duan et al. (2010) used foam as transport fluid on the particles, while we used water. This to fluids may be differently affected by the rotation on a DS.

4.2. Particle mass flow rate

The Usp is calculated based on the collection rate (Usp outlet) for both the two-phase flow with and without a DS. When the DS was added into the 5^0-inclined test section, the pressure increased. In order to make it possible to keep re-injecting particles, a new valve had to be added in top of the column. The valve could close out the hydro cyclone and made it therefore possible to measure the re-injection rate (Usp inlet) without being affected by entering particles. This change in experimental setup made it possible to easily add more particles into the flow loop, by closing both the valves, bring out the column and fill it with particles. The re-injection rate for two-phase flow with DS was calculated out from the same methods used for collection rate. In the re-injection experiment, the top valve was closed and the bottom valve was opened.

4.2.1. Collection rate

The collection rate for two-phase flow without a DS when the $C_p = 8{,}5\%$ is calculated. A plot was made to see how the Usp at outlet is affected by changing flow rates.

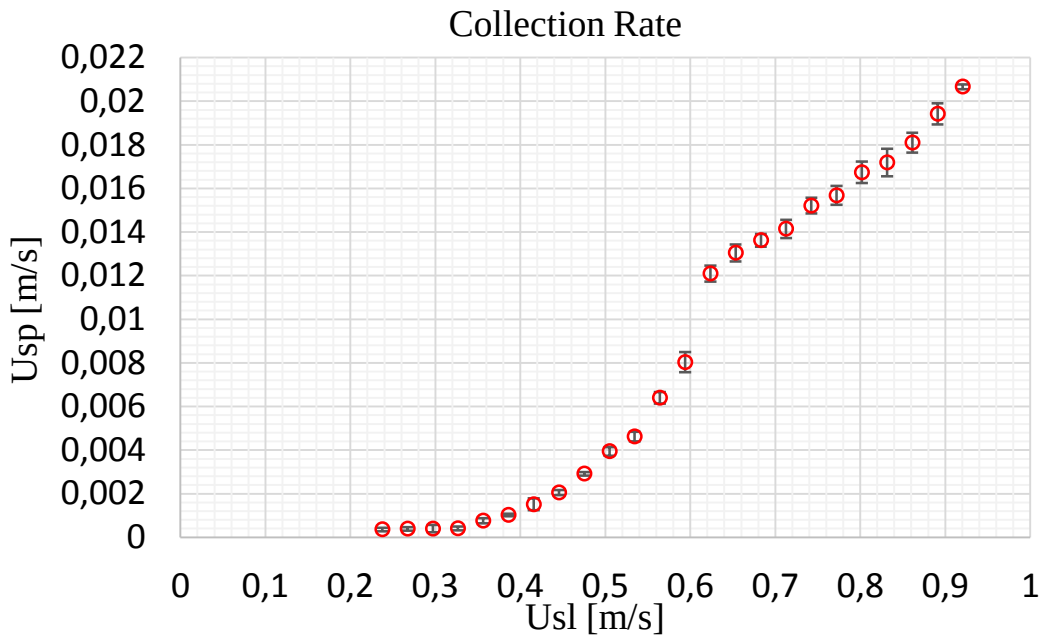

Figure 4.7: Indication on how Usp and Usl affects each other, Cp =8,5%

Figure 4.7 shows a plot of the Usp at outlet vs Usl. The Usp SD is given in the figure. The x-axis stands for the Usl and the y-axis for the Usp. Up to Usl = 0,6 m/s the curve is polynomial and for higher values of Usl the curve is linear. The plot clearly indicates that the Usl is much larger than the Usp. Figure 4.7 shows that Usp increases with increased Usl. Usl has the largest effect on the Usp, when the Usl is between $0{,}5 - 0{,}65\ m/s$.

The weight of the particles is almost the double of the water, because of that the particles falls down to the bottom of the pipe. The reason why Usp is lower than Usl is due to the particle-wall interaction that occurs at the bottom of the pipe. The Usp is lowered by the hydrodynamic interaction due to the proximity of a wall and mechanical interaction caused by contact with the wall. The result showed in figure 4.7 indicates that a Usl higher than $0{,}35\ m/s$ is needed to be able to overcome the particle-wall interaction. At a Usl larger than $0{,}65\ m/s$ the particle-wall interaction does no longer affect the Usp, Usp increases linearly with increased Usl at this moment.

4.2.2. Collection rate with a rotating drill string

The collection rate for two-phase flow with a DS when the C_p = 12,5% is calculated. A plot was made to see how the Usp at outlet is affected by different rotation speed on the DS and changing flow rates.

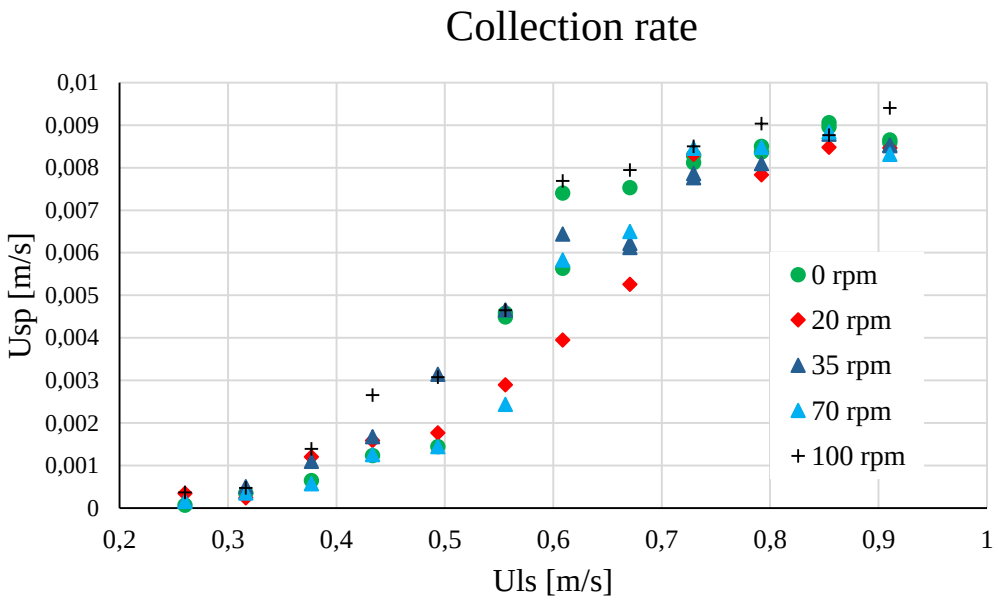

Figure 4.8: Indication on how a rotating DS affects Usp at different Usl

Figure 4.8 shows a plot of the calculated Usp at outlet vs. Usl. The plot indicates how the rotation of a DS affects the Usp. The x-axis stands for the Usl and the y-axis for the Usp. The plot shows that the rpm affects the Usp for different Usl, but no direct tendency is showing.

It is challenging to drag out any reel conclusions regarding the impact of a rotating DS since rpm = 0 shows almost the same Usp as rpm = 100. Comparing figure 4.7 with figure 4.8 indicates that the Usp decreases when the DS is added into the flow loop. This may be due to a decrease in area where the particles can travel. A larger annuls could have shown more impact of a rotating DS.

4.2.3. Re-injection rate with a rotating drill string

The collection rate for two-phase flow with a DS when the C_p = 12,5% is calculated. A plot was made to see how the Usp at inlet is affected by rotation speed on the DS and changing flow rates.

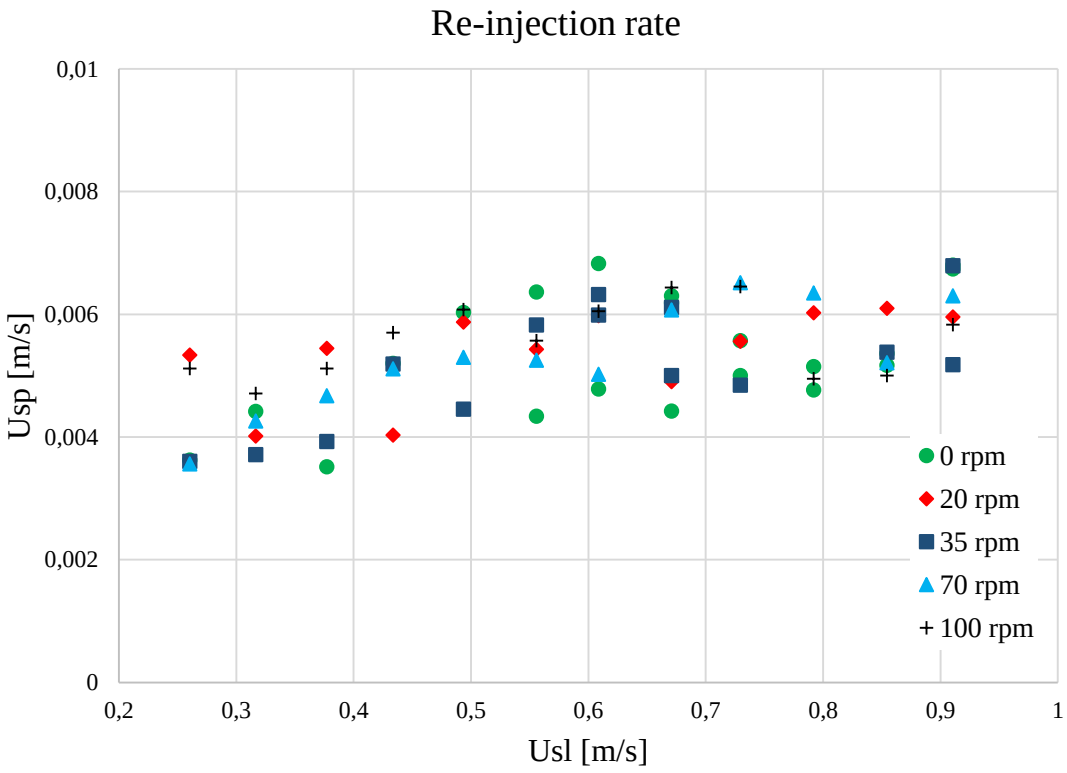

Figure 4.9: Indication on how different speed on a rotating DS effects the Usp at inlet

Figure 4.9 shows a plot of the calculated Usp at inlet for different rotation speed on the DS. The x-axis stands for the Usl and the y-axis for the Usp. The plot shows that the rpm does not affect the Usp at inlet.

The results plotted in figure 4.9 gives an indication that the Usp at inlet is constant and is not affected by Usl nor the rotation speed on the DS. The unstable measurements seems to be due to uncertainty in the measurement technique.

4.3. Flow pattern

In this master thesis, it is chosen to divide the flow patterns into 5 different categories with different sub categories, as shown below. Figure 4.10 shows what it looked like inside the pipe for different flow patterns, when the velocity is increasing. The characteristic for each of the categories were decided based on earlier studies and personal observations when running the experiments. For low velocities, more time went by before the liquid-particle flows were stabilized into the flow patterns.

- Homogenous flow: At very high flow rate, the particles are uniformly suspended in the flow by the turbulence of the carrier fluid.
- Heterogeneous flow: When the flow rate is reduced the concentration of particles will be larger in the lower section of the pipe. The particles are flowing without settling, because the lifting force is larger than the gravitational force. No bed will be formed at this range of flow rate.
- Saltating flow: Further decrease of the flow rate, the particles starts to accumulate at the bottom of the pipe, while the particles at the top of the pipe moves with a higher velocity compare to the accumulating particles.
- Moving bed: Further decrease of flow rate, the particles are moving by rolling and sliding on the surface of the formed dunes (beds).
    - Continuing moving bed (CMB): the beds are sliding into each other and making long beds (tail). The particles on the top of the dunes are dragged forward by drag and lift forces.
    - Separated moving bed (SMB), there are distances between the dunes. The particles at the surface of the dunes are moving forward the same way as CMB, while the particles inside the dunes are stationary.
- Stationary flow: At very low flow rate, the particles are settled at the bottom of the pipe, the dune is stationary while some particles on the surface of the dunes moves by rolling and sliding.

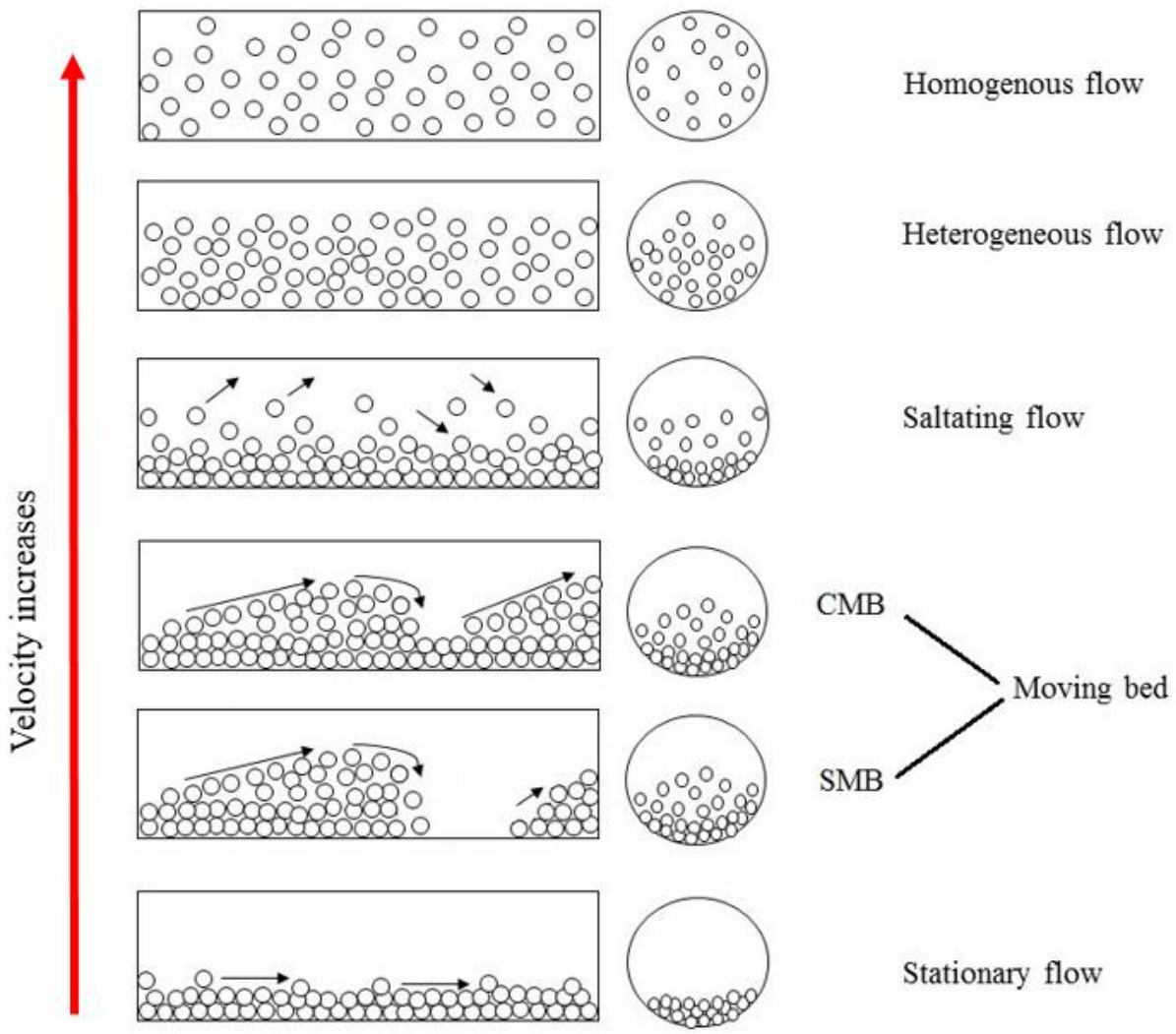

Figure 4.10: Drawing of how the particles are distributed in the pipe at different flow patterns

Deciding which flow pattern that occurred at the different velocities in the different test sections, were done by personal observation by the human eyes and can therefore differ from person to person. In this thesis it is decided to be consistent and following the description mention above. Defining when saltating flow went over to moving bed was extremely difficult, due to problems in deciding whether the particles were rolling and sliding or flowing with the flow. This might be one of the reason why Turian and Yuan (1977) decided take moving bed in under the definition of saltation in their report. Divide the flow pattern into less categories would have given a more trust worthy result, but in this thesis more details about flow pattern is wanted.

4.3.1. Flow pattern in the test sections

Each of the different flow pattern were given different symbols to indicate whitch flow pattern that were observed at different Usl. The symbols were put into the plot of all the three test sections. The overall C_p=8,5%

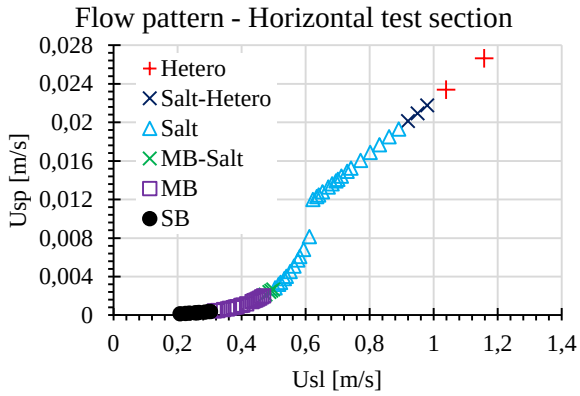

Figure 4.11: Flow pattern in horizontal test section

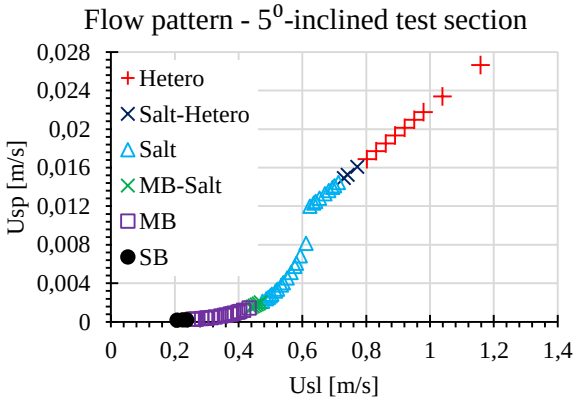

Figure 4.12: Flow pattern in 5 ^{0}-inclined test section

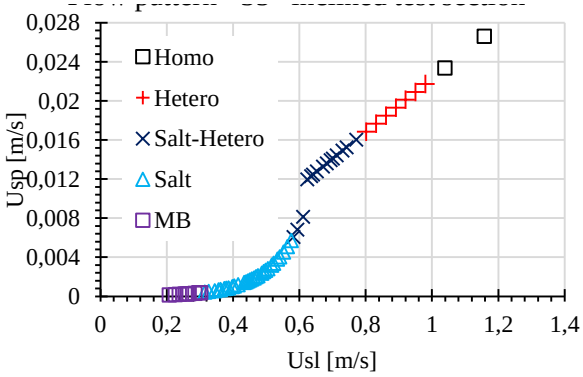

Figure 4.13: Flow pattern in 35 ^{0}-inclined test section

Figure 4.11, 4.12 and 4.13 shows how flow pattern changed with change in inclination and Usl. The x-axis stands for Usl and the y-axis for Usp. By comparing the three figures, it is possible to see that for higher inclination the transition in flow pattern was occurring at lover Usl. Figure 4.11 and 4.12 shows stationary bed at low velocity, while Figure 4.13 shows homogenous flow at high velocity. The MB observed in the 35^0-inclined testing section was acting differently than in the other test sections. In 35^0-inclined testing section the MB was sliding backwards, this observation was also mention by Li and Walker (2001). In the 35^0-inclined testing section, it was difficult to decide the flow pattern because it was always settling faster in the top than at the bottom of the inclined pipes. The result presented in figure 4.13 is out from observations done at the middle of the 35^0-inclined testing section.

4.3.2. Flow patterns impact on differential pressure

To get an indication on whether flow patterns affect pressure drop or not, DP were plotted together with the corresponding flow pattern for three of the test sections. Images are put into the plots, to make an illustration on what the flow patterns look like in the different test sections. It is chosen to not take the transition zone into the plot and instead set larges lines when we are shore that the new flow pattern has started. Dotted lines is sat to indicate which kind of moving bed that occurs where, when we have a moving bed pattern.

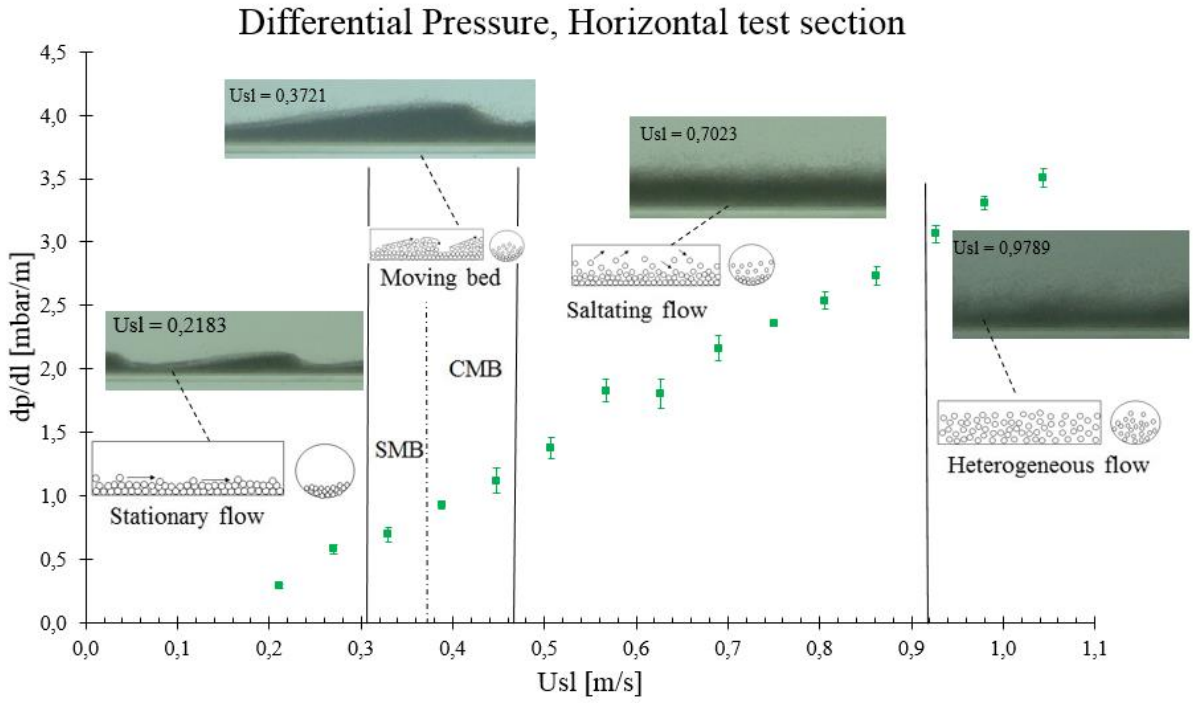

Figure 4.14: DP and the corresponding flow patterns with image and illustration for the horizontal test section

Figure 4.14 shows the plot of DP with SD and the corresponding flow patterns for the horizontal test section. The x-axis stands for Usl and the y-axis for DP over the length of the test section. The images are pictures of the pipe taken from the side, each of the images shows the observed flow pattern inside the pipe for a given Usl. On the images, it is possible to see how the distribution of particles changes with different flow patterns. The DP plot in figure 4.14 indicates that flow pattern has no effect on DP in the horizontal test section. The DP is increasing linearly with increased Usl. At the beginning of the saltating flow a small jump in DP is shown, this jump can be caused by change in local C_p or mistakes in the measurements, even though small uncertainties are shown.

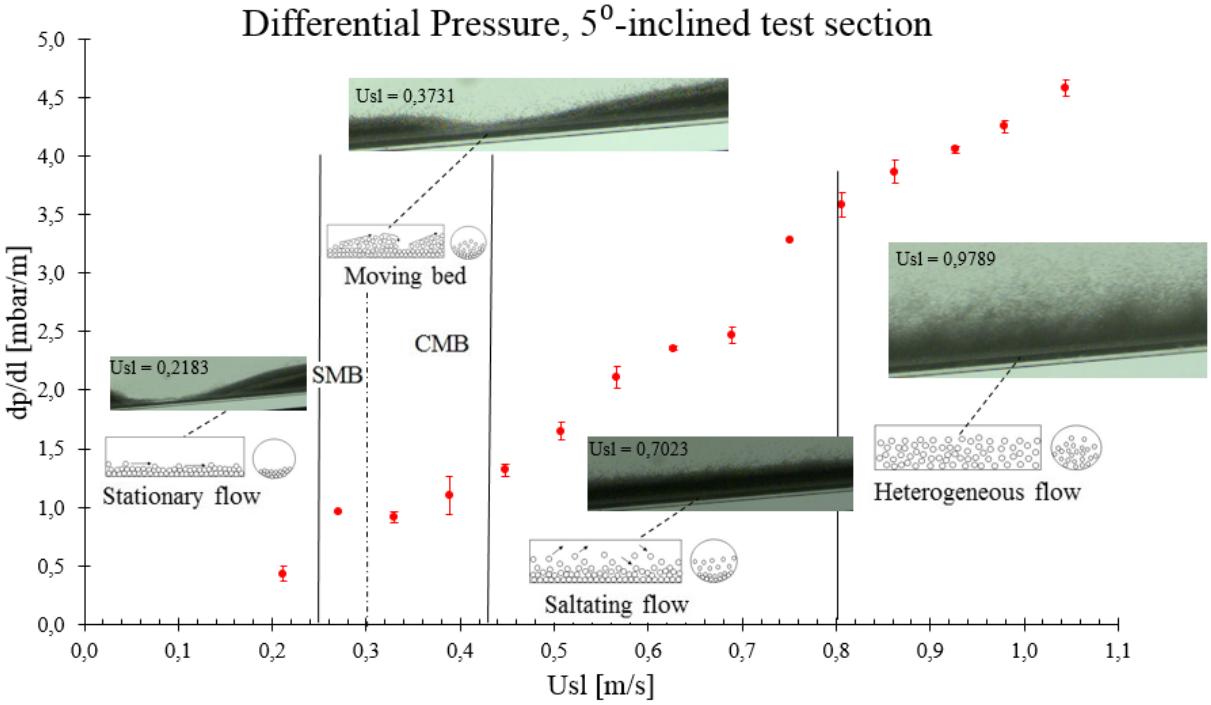

Figure 4.15: DP and the corresponding flow patterns with image and illustration for the 5°-inclined test section

Figure 4.15 shows the plot of DP with SD and the corresponding flow patterns for the 5°-inclined test section. The x-axis stands for Usl and the y-axis for DP over the length of the test section. The images are pictures of the pipe taken from the side at different flow rates. In the images, it is possible to see how the distribution of particles changes at different flow pattern.

The DP plot in figure 4.15 indicates flow patterns effect on DP in the 5°-inclined test section. The DP makes a jump when the flow pattern goes from stationary flow to moving bed, before it goes back down and settles to a linear increase in DP. The linear increase in DP changes when the transition zone from saltating flow to heterogeneous flow is reached, then the pressure goes down, before is goes up and stabilizes back to a linear increase again.

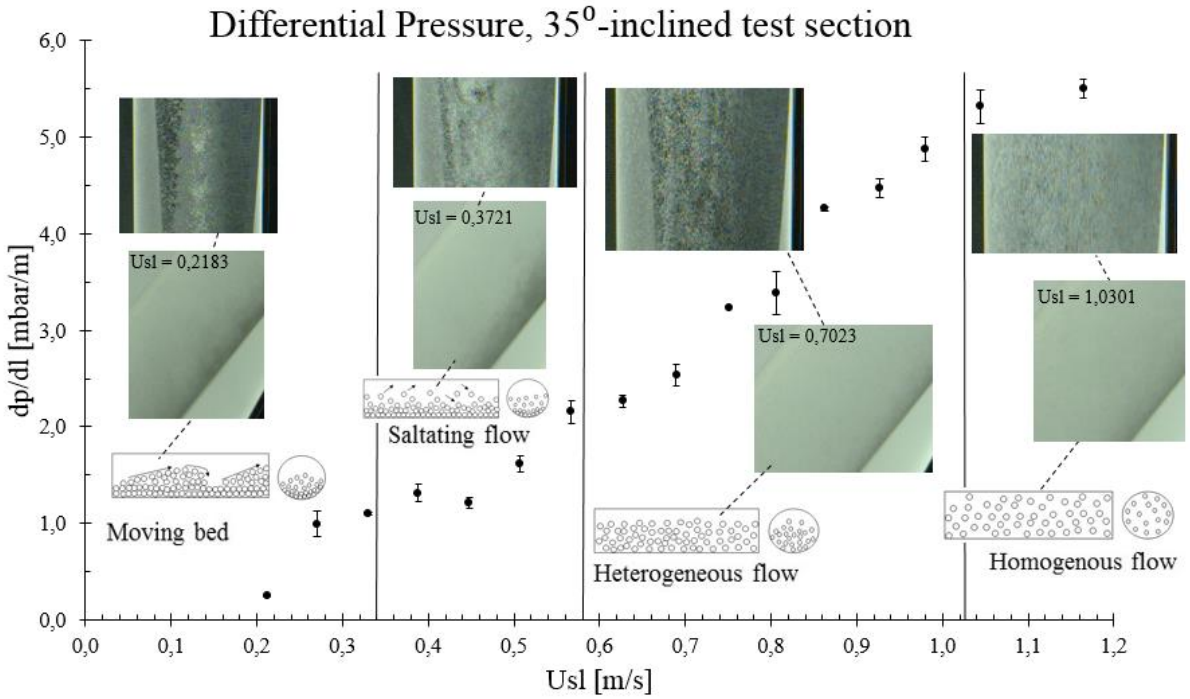

Figure 4.16: DP and the corresponding flow patterns with image and illustration for the 35 ^{0}-inclined test section

Figure 4.16 shows the plot of DP with SD and the corresponding flow patterns for the 35°-inclined test section. The x-axis stands for Usl and the y-axis for DP over length of the test section. Two different types of images are added into plot, to make an illustration on how the flow looks for different flow patterns. The dark images are taken from below to show how the particles are settling. The bright image is taken from the side of the pipe, to show the distribution of particles in the pipe. In the images, it is possible to see how the distribution of particles changes for different flow rates.

The DP plot in figure 4.16 indicates that flow patterns effect on DP in the 35°-inclined test section. The DP makes a jump right before the flow pattern goes from moving bed to saltating flow, the DP keeps increasing with the Usl until the middle of saltating flow area, where the pressure drops again. From the drop in the middle of the saltating flow area and until middle of the heterogeneous flow area the DP increases with the Usl. In the middle of the heterogeneous flow area, the pressure drop increases and keeps following a stable linear increase.

Out from figure 4.15 and 4.16 it is possible to see two suddenly changes in DP in each of the plots, these changes do not happen at the same velocities as changes in flow patterns occur. The reason why changes in flow patterns and DP does not happen at the same Usl, might be mistakes

in the DP measurements or that it is the transition zones that affects the DP. The fall out might have been different if a different length on the test section, Cp or a different size on the pipe was applied. For inclined pipes is possible to agree with Pinchas Doron and Barnea (1995) conclusion that flow pattern and DP affects each other. Based on our observation on flow pattern and measured DP it is challenging to agree with H. Rabenjafimanantsoa (2007) conclusion that DP can be used to identification of flow pattern. In our cases the flow pattern looked the same before and after a jump or drop in DP.

4.3.3. Different rotation speed on a rotating drill string

The change in flow patterns due to different rotation speed on the DS were observed in the 5°-inclined test section. The overall C_p = 12,5%.

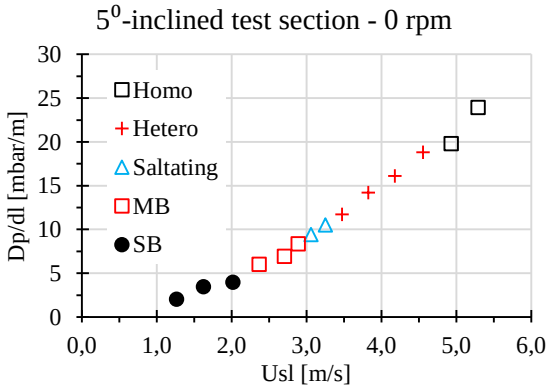

Figure 4.17: Flow pattern in 5 ^{0}-inclined test section with a rotation = 0 rpm on the DS.

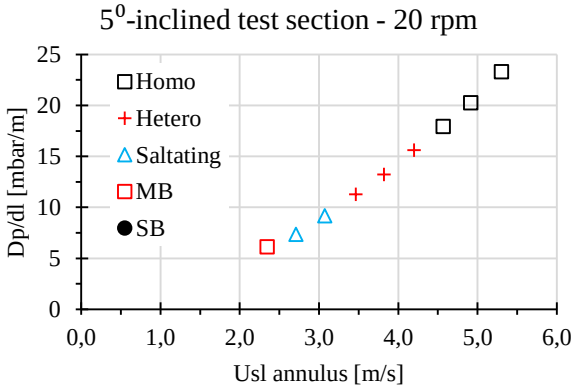

Figure 4.18: Flow pattern in 5 ^{0}-inclined test section with a rotation = 20 rpm on the DS

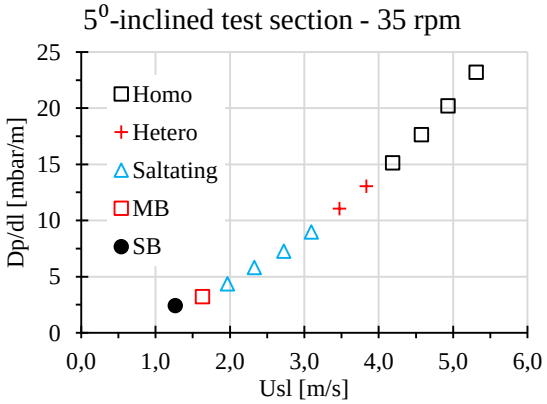

Figure 4.19: Flow pattern in 5 ^{0}-inclined test section with a rotation = 35 rpm on the DS

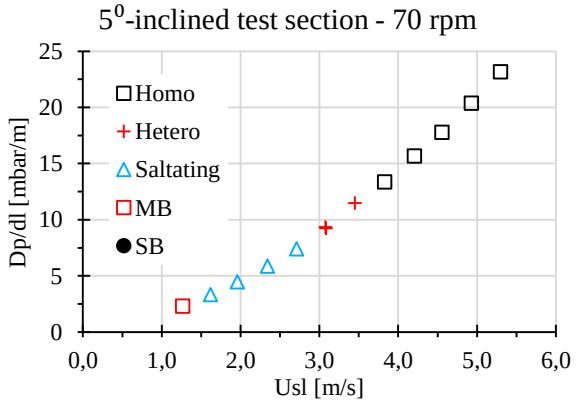

Figure 4.20: Flow pattern in 5 ^{0}-inclined test section with a rotation = 70 rpm on the DS

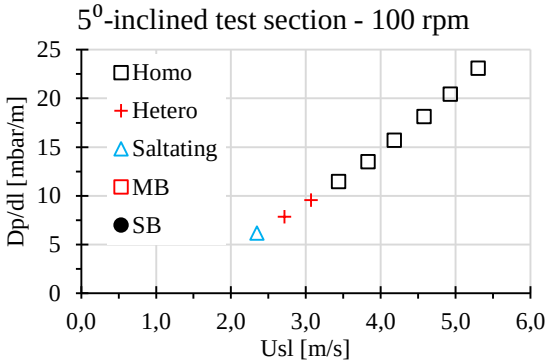

Figure 4.21: Flow pattern in 5 ^{0}-inclined test section with a rotation = 100 rpm on the DS

Figure 4.17 to 4.21 shows how the flow patterns and DP change due to different rotation speed on the DS. The x-axis stands for Usl (Usl in annulus for figure 4.18) and the y-axis for DP over the length of the test section. Comparing the five figures, gives an indication that the rpm affects the flow patterns but not the average DP. The figures indicates that the largest change in flow pattern due to different rotations speeds happens at 0 rpm to 35 rpm. Figure 4.19 shows that the saltation flow pattern happens at a much lower Usl than in figure 4.17. Increased rpm leads to lower Usl needed to reach each of the flow patterns.

The figures give a clear indication of that rotation on DS affects the flow patterns and that the effect is largest at rpm 0 to rpm 30, after that the rpm still affects, but the effect is not increasing in the same speed. A faster change between flow patterns before reaching homogeneous flow, indicates the particles get better distributed in the flow the higher the rotation speed on the drill string is. For the selected flow rates in this experiments, the stationary bed was not observed when the rotation speed on the DS was above 70 rpm.

4.4. Velocity profile

The measurement techniques, PIV and UVP were used to get an indication on the velocity profile in both single- and two-phased flow. The velocity profiles are given in the flow direction, by u and v component. The u component is the axial velocity is in the same direction as the flow. The v component is the radial/lift velocity in the direction vertically on the flow direction. The PIV measurement technique is applied in horizontal, 5^{0}- and 35^{0}-inclined test section while the UVP measurement technique is only used in the 5^{0}-inclined test section for single-phase flow due to problems with moving the UVP equipment.

4.4.1. Single-phase flow

The single-phase water flow was used to check if PIV and UVP gave the same velocity profiles. Since UVP is one-dimensional it only gives the velocity in x-direction, this has to be taken into account when comparing the results. The UVP equipment should have been installed in the horizontal test section, to give an as accurate comparison as possible. In the results presented for single-phase flow, the U component is given in horizontal direction for all the cases. The distance is given as the cross section of the pipe and is measured from the top to bottom of the pipe.

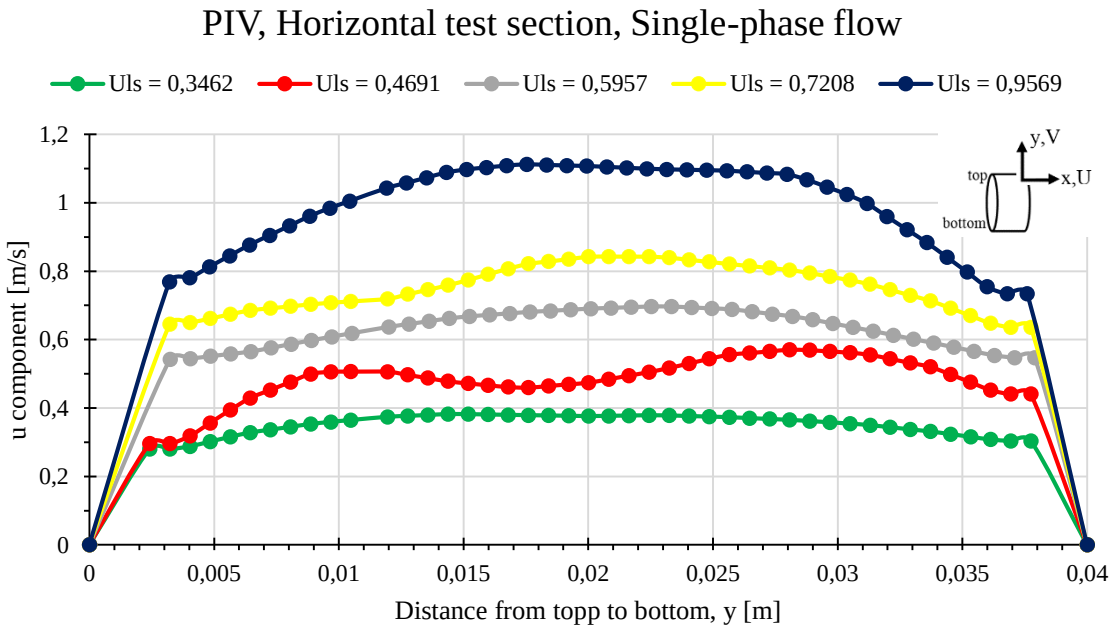

Figure 4.22: Velocity profile for different Usl, made by using PIV for the horizontal test section

Figure 4.22 shows a plot of the velocity profile measured by using PIV for different velocities in the horizontal test section. The x-axis stands for distance and y-axis for velocity in flow direction. The plot shows no detection of particles in the boundary layer, close to the wall. The wave shape on the curves for Usl = 0,4691 and Usl = 0,7208 is most likely due to lack of detected seeding particles.

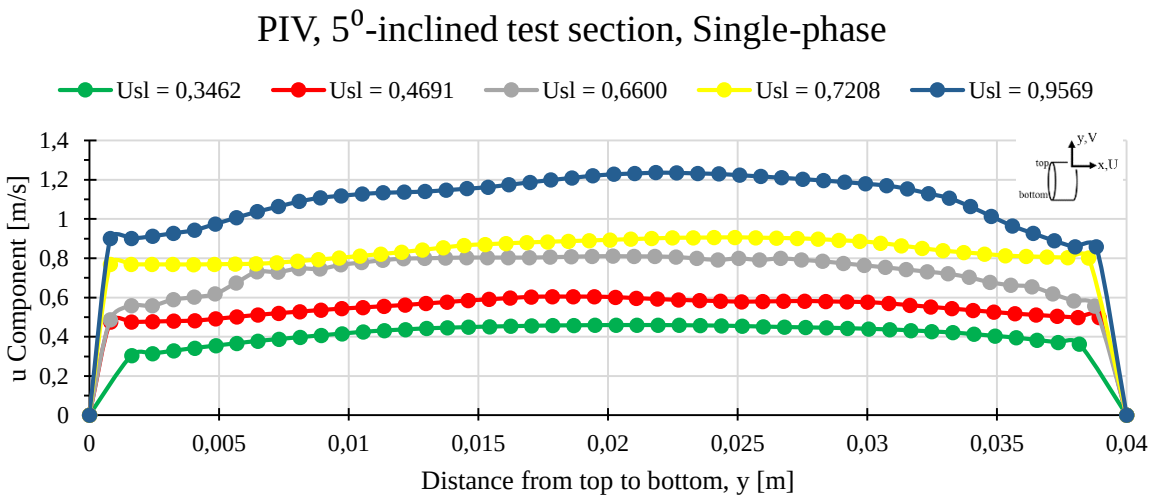

Figure 4.23: Velocity profile for different Usl, made by using PIV for the 5 ^{0}–inclined test section

Figure 4.23 shows the plotted velocity profile in the horizontal direction measured by using PIV for different velocities in the 5°-inclined test section. The x-axis stands for distance and y-axis for velocity in horizontal direction. The plot shows no detection of particles in the boundary layer, close to the wall. The wave shape on the curve for Usl = 0,6600 is most likely due to lack of detected seeding particles.

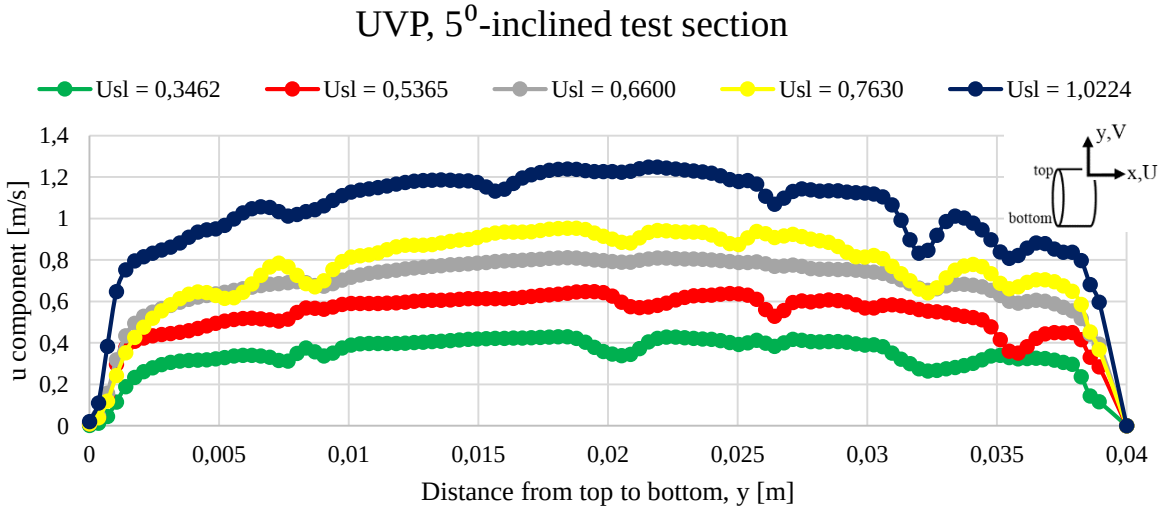

Figure 4.24: Velocity profile for different Usl, made by using UVP for the 5 ^{0}–inclined test section

Figure 4.24 shows the plotted velocity profile in the horizontal direction measured by using UVP for different velocities in the 5°-inclined test section. The x-axis stands for distance and y-axis for velocity in horizontal-direction. The wave shape on the curves presented in figure 4.24 is most likely due to lack of detected seeding particles. The UVP detects more seeding particles than PIV in the boundary layer.

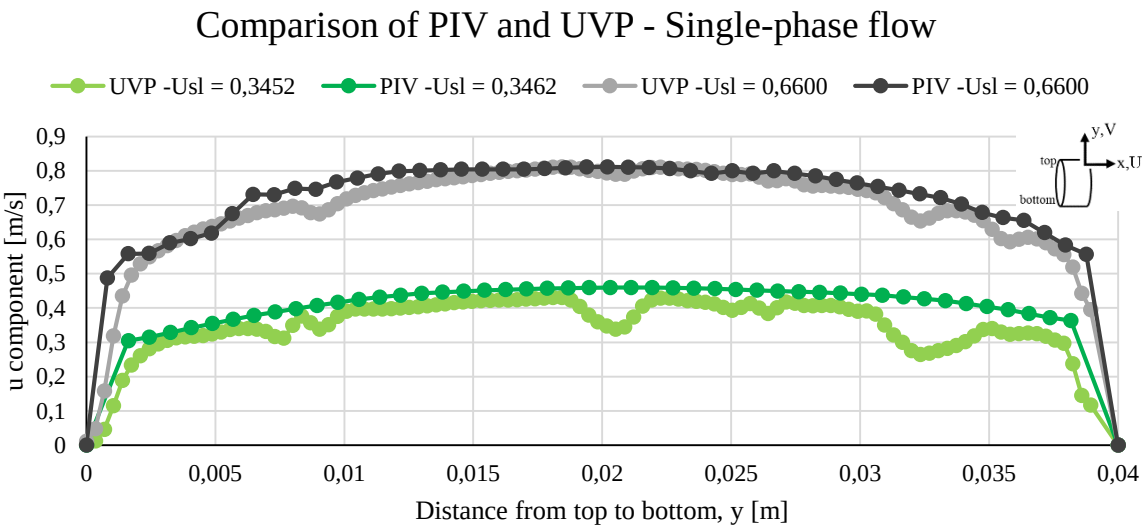

Figure 4.25: Comparison of Velocity profile made by using PIV and UVP for 5 ^{0}–inclined test section at different Usl

Figure 4.25 shows the plotted velocity profiles in the horizontal direction measured by using PIV (dark colure) and UVP (bright colure) for two different velocities in the 5°-inclined test section. The x-axis stands for distance and y-axis for velocity in horizontal direction. The plot shows no detection of particles in the boundary layer, close to the wall. The wave shape on the curves presented in figure 4.25 is most likely due to lack of detected seeding particles.

Figure 4.25 indicates that PIV measures a little higher velocity profile than UVP. By the looks on the curves, it looks like there were some noises in the UVP data because of lack of seeding particles. UVP detects more particles in the boundary layer than PIV. Problems with detecting seeding particles in the boundary layer when using PIV might by because of problems with reflections on the surface of the pipe. The result shows that PIV and UVP are in good agreement and both detecting similar velocity profiles.

4.4.2. Two-phase flow

In two-phase flow, only the PIV measurement technique was applied since this method can give results in two-dimension and out from the single-phase measurements it is shown that PIV gives close to the same result as UVP. The velocity profile for two-phase flow with C_p=8,5% is presented by u and v component, the u component is always given in the flow direction and the v component in the direction vertically on the flow direction. The figures indicates particle velocity, velocity = 0 can indicate lack of seeding particles or SB. The distance is given as the cross section of the pipe and is measured from the top to bottom of the pipe.

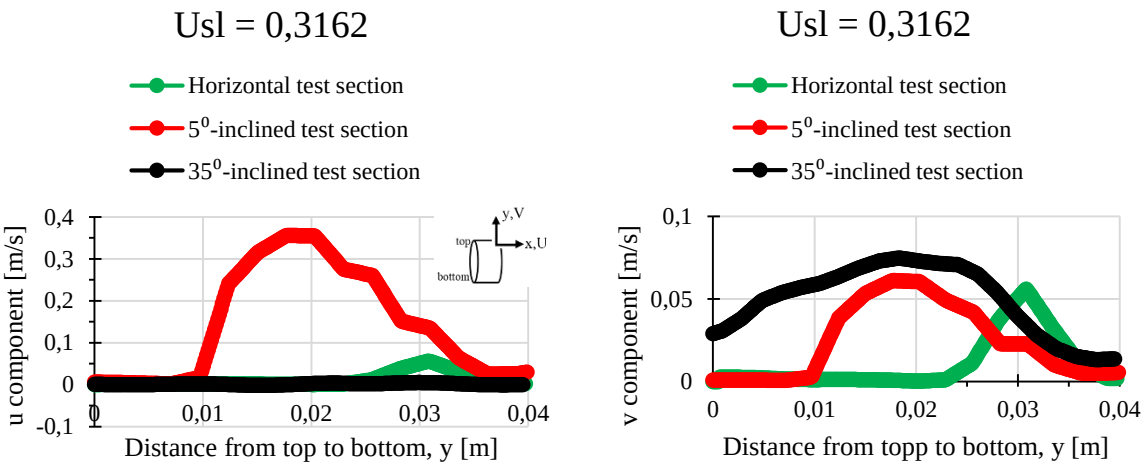

Figure 4.26: u and v component for Usl = 0,3162 for the three different test sections

Figure 4.26 shows plots of the u and v component in flow direction when the Usl = 0,3162 for the three different test sections. The x-axis stands for distance from top of the pipe to the bottom of the pipe and y-axis for the velocity in u/v direction. The small top in the horizontal test section both for u and v component, indicates low velocity on the particles. These velocities are most likely through rolling and lifting on the top of a bed, due to no detection of particles at the bottom of the pipe. The 5°-inclined test section indicates an increase in velocity towards the middle of the pipe for both u and v component. These increased velocity towards the middle of the pipe indicates a MB moving with a higher speed than the MB in the horizontal test section. The 35°-inclined test section indicates velocity through lifting.

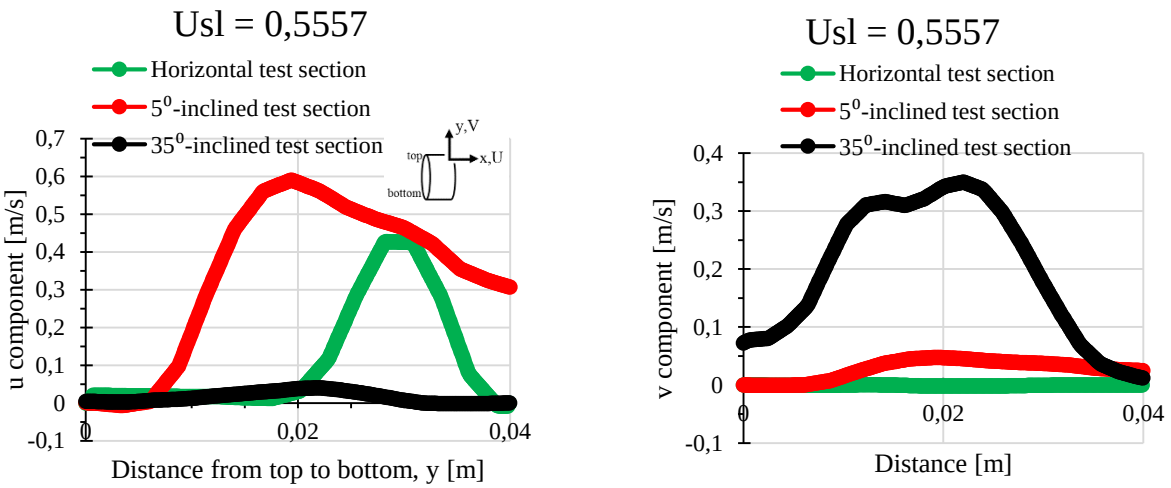

Figure 4.27: u and v component for Usl = 0,5557 for the three different test sections

Figure 4.27 shows plots of the velocity in flow direction when the Usl = 0,5557 for the three different test sections. The x-axis stands for distance from top of the pipe to the bottom of the pipe and the y-axis for velocity in u/v direction. Figure 4.27 shows that the velocity is dominant in one direction for all test sections. For the horizontal and 5°-inclined test section the u component has increased which indicates a higher axial velocity when Usl increase. The 35°-inclined test sections has an increase in lift velocity.

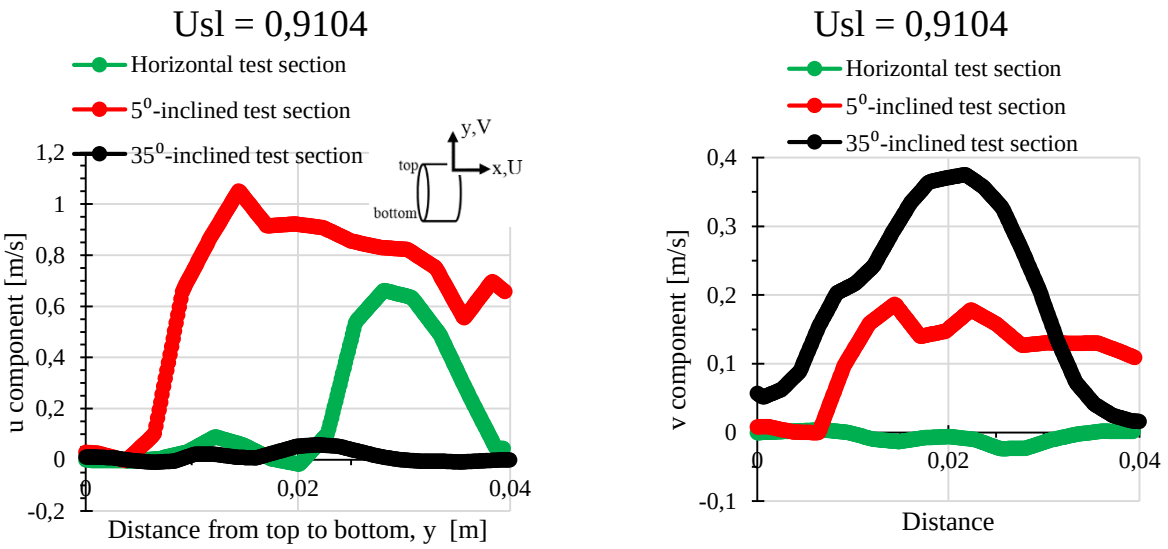

Figure 4.28: u and v component for Usl = 0,9104 for the three different test sections

Figure 4.28 shows plots of the velocity in flow direction when the Usl = 0,9104 for the three different test sections. The x-axis stands for distance from top of the pipe to the bottom of the pipe and the y-axis for velocity in u/v direction. Figure 4.28 indicates that the axial velocity is dominant for the horizontal test section. The 5°-inclined test section shows velocity in both direction, but the axial velocity direction is dominant. The lift velocity is still dominant in the 35°-inclined test sections, but the curves indicates that there are some positive movements of particles in the flow direction as well.

The velocity profiles gives a good indication of the particles velocities at different flow rates as well as an indication on how the inclination on the pipe affects the movement of particles. Comparing figures 4.26, 4.27 and 4.28 gives an indication that the particles are best distributed and have the largest axial velocity in the 5°-inclined test section at high Usl. The axial velocity is lowest in the 35°-inclined test section for low Usl. Low particle velocity in flow direction indicates bad particles transport, and I can based on my results agree with Li and Walker (2001) conclusion that particles transport is most difficult at low velocity and in pipes with inclination around 40°.

4.4.3. Two-phase flow, with a rotating drill string

From earlier experiments in this thesis it is indicated that the larges change is between rpm 0-35, in this section it is chosen to present the result for rpm 0, 35, 70 and 100. When the DS is rotating, the eccentricity of the DS has to be taken into account for better understandings of the measured velocities. The eccentricity is an elliptic movement on the DS that can affect the distribution of particles. The results presented is from the 5°-inclined test section. In the 5°-inclined test section, the ribbons glued on the DS are visible. These ribbons made problems with detecting particles in PIVlab and it is therefore chosen to present the velocity profile found at the upper section of the 5°-inclined pipe, where the ribbons do not exist. A comparison of the velocity profiles measured in the two different sections on the 5°-inclined pipe are presented. The presented velocity profile is decomposed into u and v component. The u component is given in the flow direction and the v component in the direction vertically on the flow direction. The results will give an indication on how different rotation speed on the DS and flow rates affects the velocity profile. The distance is given as the cross section of the pipe and is measured from the top to bottom of the pipe.

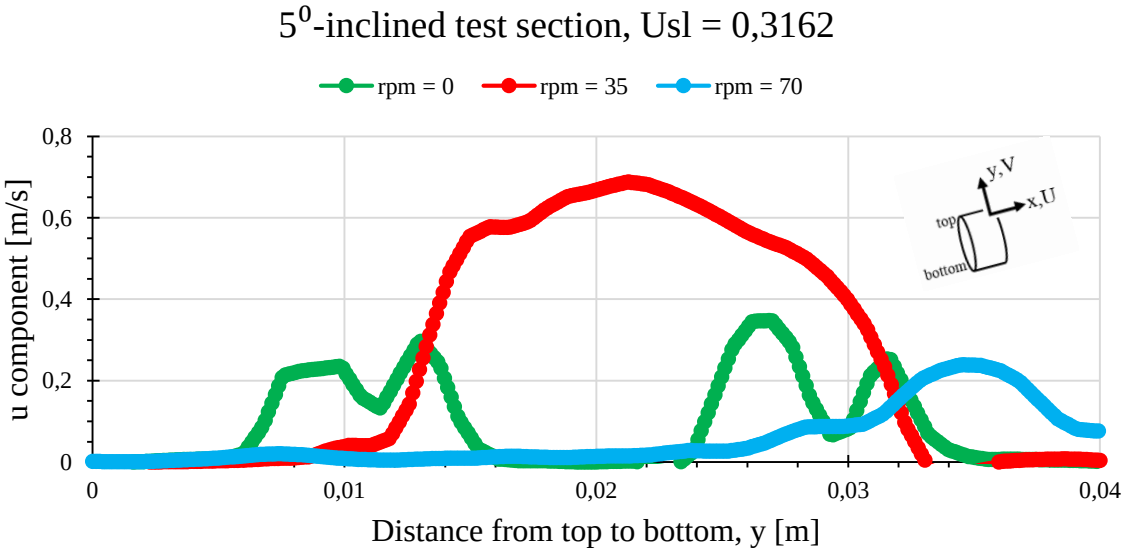

Figure 4.29: Velocity measured in the flow direction with constant Usl =0,3162 and different rotation speed on the DS, for the 5 ^{0}-inclined test section (Cp =12,5%)

Figure 4.29 shows a plot of the measured velocity in flow direction. The x-axis shows the distance from top to the bottom of the pipe and the y-axis the velocity in the flow direction. The lack of particles in the middle of the green curve for 0 rpm, is where the black ribbon is placed, the tops indicates the movements of particles and the downward peaks is most likely lack of

particles. The ribbons does not affect the curve showing 35 rpm, because the picture is taken at a time when the ribbon was not showing. The sides on the curve showing 35 rpm indicates no detection of moving particles, for the left side this indicates no particles in the flow and for the right side this indicates SB. The curve showing 70 rpm is affected of the ribbons, in this case the pictures are taken when both the ribbons are showing, movements of particles are only showing on the right side and indicates a moving bed.

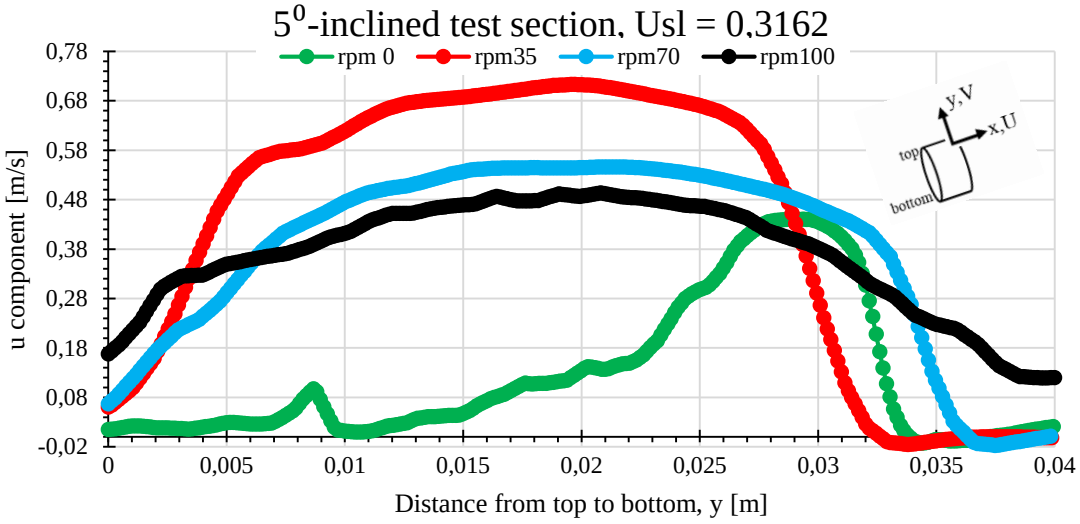

Figure 4.30: Velocity measured in flow direction with constant Usl =0,3162 and different rotation speed on the DS, for the 5 ^{0}-inclined upper section, (Cp =12,5%)

Figure 4.30 shows a plot of the measured velocity in flow direction. The x-axis shows the distance from top to the bottom of the pipe and the y-axis the velocity in the flow direction. Figure 4.30 indicates a more uniformly distribution of particles when the rpm increases. The first effect showing when rpm increases is that the particles velocity increases and when the rpm increases even more, particles goes towards a more uniform distribution in the flow. The low velocity at the bottom of the pipe indicates SB/MB, the accumulated particles disappears when the rpm increases to 100 at Usl = 0,3162. Figure 4.30 indicates that the height of the SB is higher at 35 rpm than 0 rpm. At 0 rpm, the DS is situated at the bottom of the pipe, the SB/MB get affected by the weight of the pipe. The DS pushes the particles up and into the wall, the bed layer gets thinner on the sides and it is then easier for the particles to be dragged with the flow. The pictures selected out at 35 rpm is taken when the ellipse of the DS is on its way downwards, which is most likely the reason why the SB is higher at 35 rpm than 0 rpm.

By comparing figure 4.29 and figure 4.30 it is possible to see equal tops on the curves, but the curves showing 0 rpm and 70 rpm looks a lot different when the black ribbons is not affecting the detection of particle movements. The upper section gives more thrust worthy result due to equal visual observations and no ribbons affecting the detection of particle movements in flow direction. The 5°-inclined upper section is therefore used for presenting the velocity in flow direction for the rest of the different flow rates.

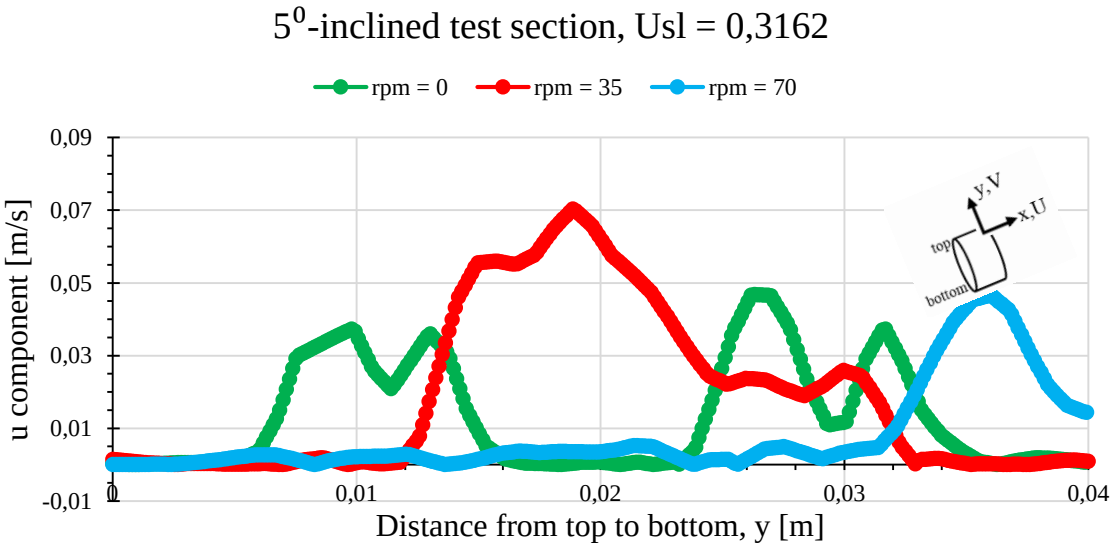

Figure 4.31: Velocity measured in direction vertically to the flow direction with constant Usl =0,3162 and different rotation speed on the DS, for the 5 ^{0}-inclined test section, (Cp =12,5%)

Figure 4.31 shows a plot of the measured velocity in the direction vertically on the flow direction. The x-axis shows the distance from the top to the bottom of the pipe and the y-axis the velocity in the direction vertically to the flow direction. Figure 4.31 shows the same problems with detection in the area where there are ribbons as figure 4.29.

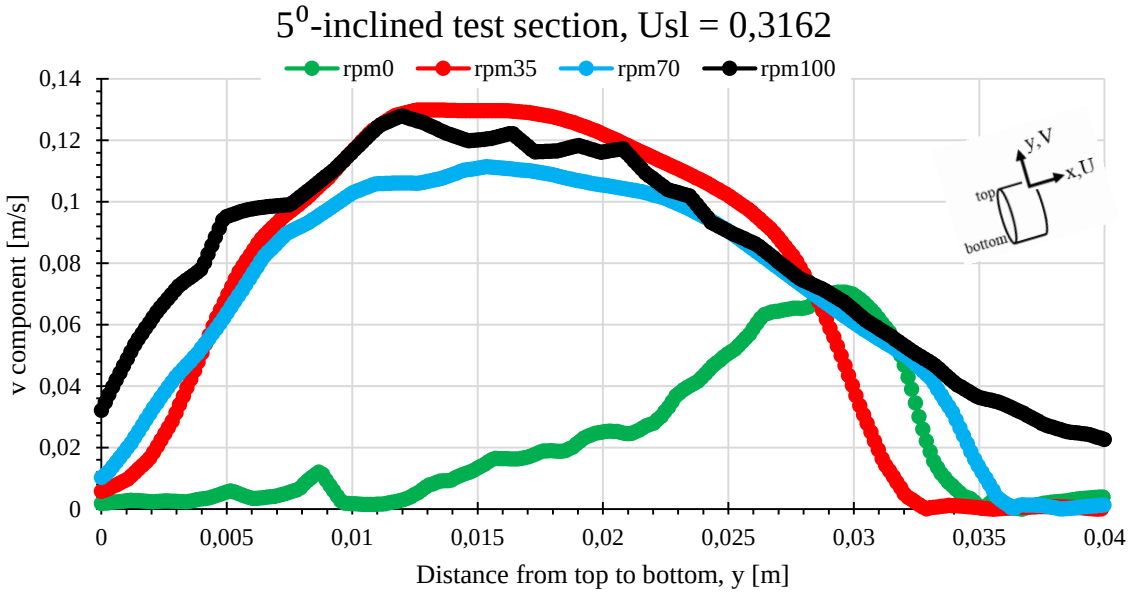

Figure 4.32: Velocity measured in direction vertically to the flow direction with constant Usl=0,3162 and different rotation speed on the DS, for the 5 ^{0}-inclined upper section, (Cp =12,5%)

Figure 4.32 shows a plot of the measured velocity in the direction vertically on the flow direction. The x-axis shows the distance from the top to the bottom of the pipe and the y-axis the velocity in the direction vertically to the flow direction. Figure 4.32 shows that the rpm has a large effect on lift velocity. The lift velocity starts to increase at 35 rpm, then it decreases and shows a more uniformly distribution of particles at 70 rpm before the lift velocity increases again for 100 rpm. At 100 rpm there are no indications of stationary bed for Usl = 0,3162.

Comparing figures 4.31 and 4.32 with the images used to create a velocity profile gives good indications that the measured velocity in the 5°-inclined upper section fits well with the visual observations. The 5°-inclined upper section gives good indications for velocity in the direction vertically on the flow and is used to present the velocity for the rest of the different flow rates.

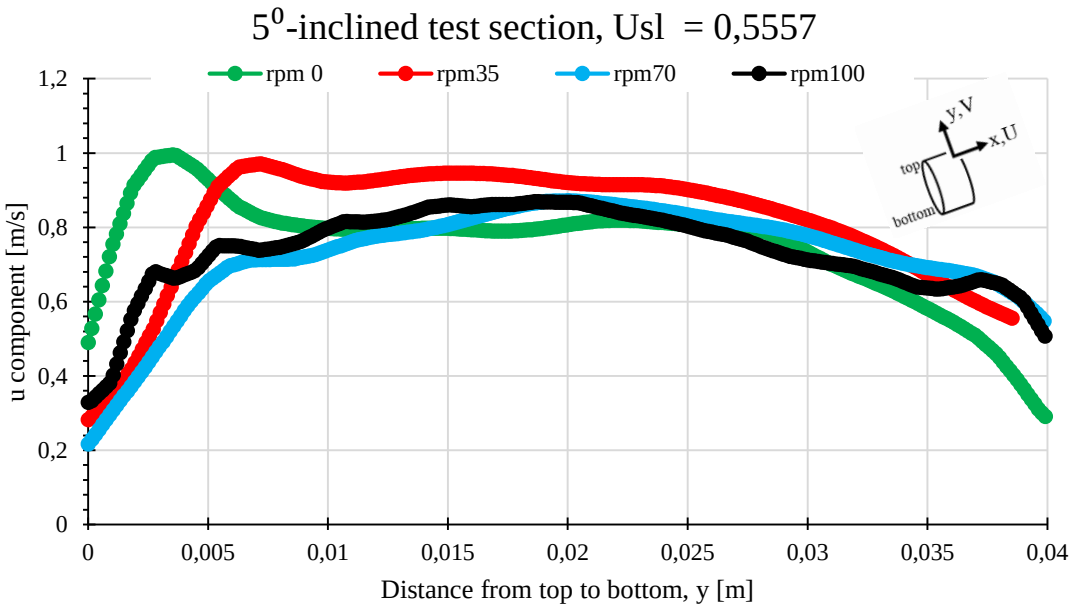

Figure 4.33: Velocity measured in flow direction with constant Usl =0,5557 and different rotation speed on the DS, for the 5 ^{0}-inclined upper section, (Cp =12,5%)

Figure 4.33 shows a plot of the measured velocity in flow direction. The x-axis shows the distance from top to the bottom of the pipe and the y-axis the velocity in the flow direction. Figure 4.33 indicates small changes one the axial velocity due to increased rpm. The changes in the boundary layer is affected by the eccentricity of the DS, whether the selected images are taken when the DS moves downwards or upwards. The bump spotted in the curves at 0 rpm and 35 rpm is most likely due to a large flow area when the DS is at the bottom of the pipe.

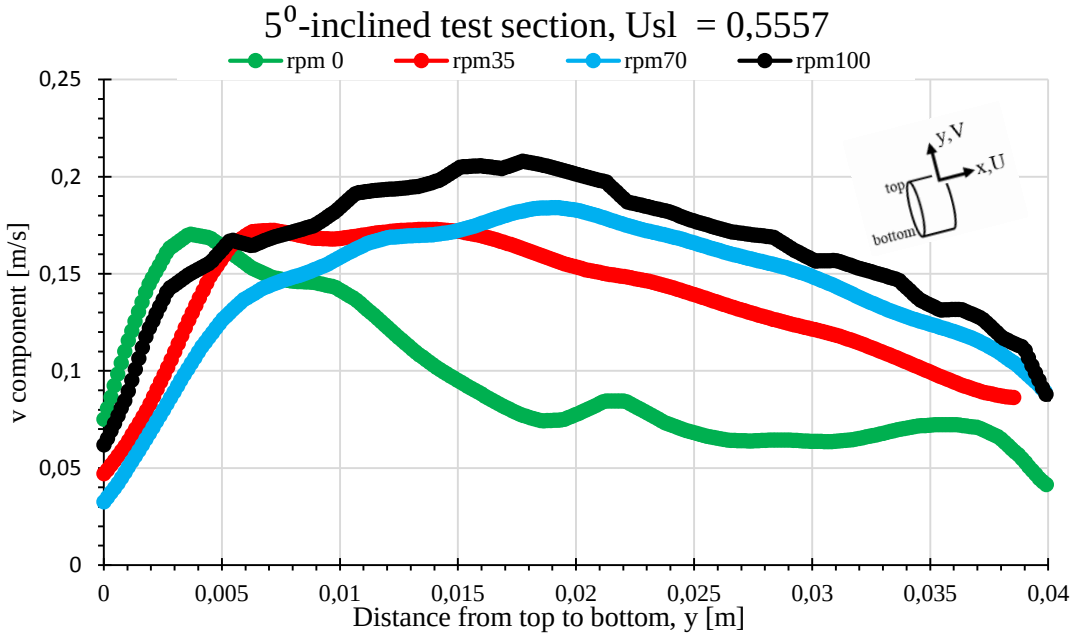

Figure 4.34: Velocity measured in direction vertically to the flow direction with constant Usl=0,5557 and different rotation speed on the DS, for the 5 ^{0}-inclined upper section, (Cp =12,5%)

Figure 4.34 shows a plot of the measured velocity in the direction vertically on the flow direction. The x-axis shows the distance from the top to the bottom of the pipe and the y-axis the velocity in the direction vertically to the flow direction. Figure 4.34 indicates that the rpm has a large effect on the lift velocity, higher rpm gives an increase in lift velocity and a more uniform distribution of the particles. The high lift velocity at 0 rpm in the top of the pipe is due to larger flow area when the DS is situated at the bottom of the pipe.

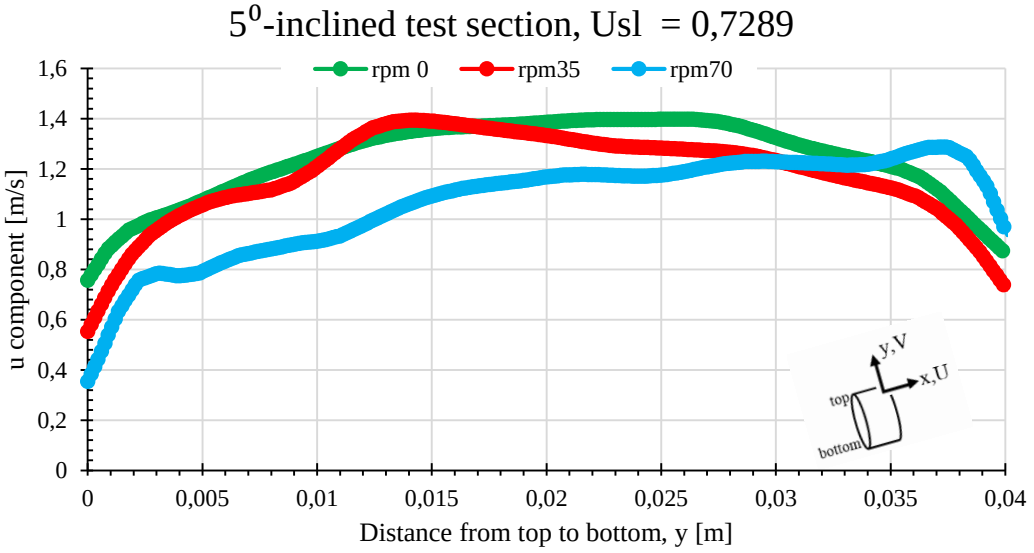

Figure 4.35: Velocity measured in flow direction with constant Usl =0,7289 and different rotation speed on the DS, for the 5 ^{0}-inclined upper section, (Cp =12,5%)

Figure 4.35 shows a plot of the measured velocity in flow direction. The x-axis shows the distance from top to the bottom of the pipe and the y-axis the velocity in the flow direction. Figure 4.35 indicates small changes on the axial velocity due to increased rpm. The changes in the boundary layer is affected by the eccentricity of the DS and is therefore affected by whether the DS is moving downwards or upwards. The bump spotted in the curve at 70 rpm at the bottom of the pipe is because the particles getting a larger flow area when the DS is moving upwards

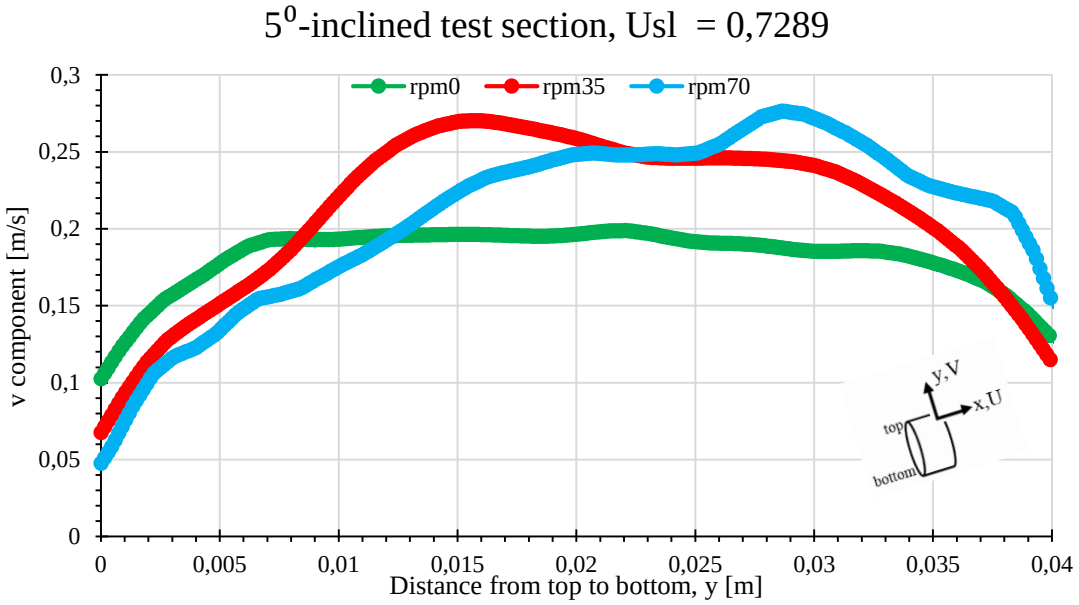

Figure 4.36: Velocity measured in direction vertically to the flow direction with constant Usl=0,7289 and different rotation speed on the DS, for the 5 ^{0}-inclined upper section, (Cp =12,5%)

Figure 4.36 shows a plot of the measured velocity in the direction vertically on the flow direction. The x-axis shows the distance from the top to the bottom of the pipe and the y-axis the velocity in the direction vertically to the flow direction. Figure 4.36 shows that the 35 rpm has a large effect on the lift velocity, the affect only increases in the bottom of the pipe for higher rpm. In the boundary layer on the top of the pipe, 0 rpm gives the highest velocity and shows a uniform distribution of the axial velocity.

Figures showing the velocity profile for three different flow rates indicates that effect of the rpm depends on the flow rate. For axial velocity, 35 rpm gives the largest effect, the effect decreases with increased flow rate. Increased rpm gives less SB and a more unformal

distribution of axial velocity. For the lift velocity, higher rpm gives higher lift velocity, the effect of the rpm decreases with increased flow rate.

Based on comparison of image and given velocity profile it is possible to use PIV as a tool to decide flow patterns. PIV gives a good indication on movement of particles that can be difficult to see with the human eye. By using PIV it might be possible to find the accurate velocity for different flow patterns and check if this velocity is equal to the velocity when the increase in DP suddenly makes a jump.

4.5. Height of bed dunes

It took time before the dunes was fully developed and observation of the dunes giving an indication that a tall dune where followed by a smaller dune, it was therefore important to take the images of the highest dune at each of the flow rates. The height of the bed dunes was measured for a large amount of images. The height was measured from the bottom of the pipe to the surface of the bed dunes at the highest point on the bed dunes. The height of the dunes was measured for two-phase flow with and without a rotating DS.

4.5.1. Two-phase flow

In the two-phase flow the Cp = 8,5%.

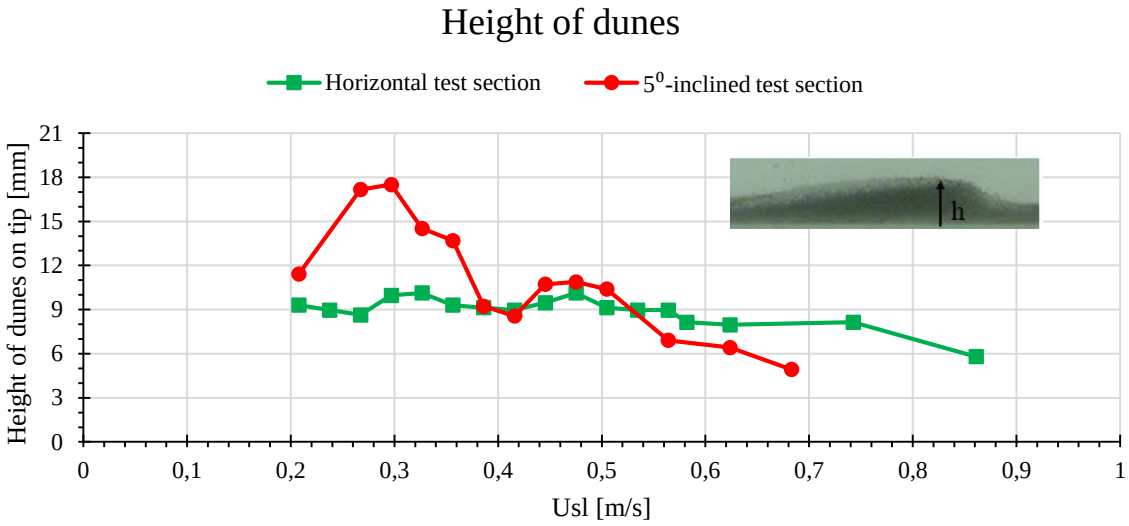

Figure 4.37: Height of dunes in two-phase flow for different Usl, the bumps indicates changes in flow patterns, (Cp =8,5%)

Figure 4.37 shows the height of the dunes at different flow rates. The x-axis stands for Usl and y-axis for the measured height of the dunes. Figure 4.37 indicates higher dunes in the 5°-inclined test section at low velocities. The curves for horizontal and 5°-inclined test section shows bumps indicating changes in flow patterns, the density on the top layer decreases and more particles are pushed up and making the bed height increase. The images resolution is too low to detect the change in density.

4.5.2. Two-phase flow, with a rotating drill string

In the two-phase flow with a rotating DS the Cp = 12,5%.

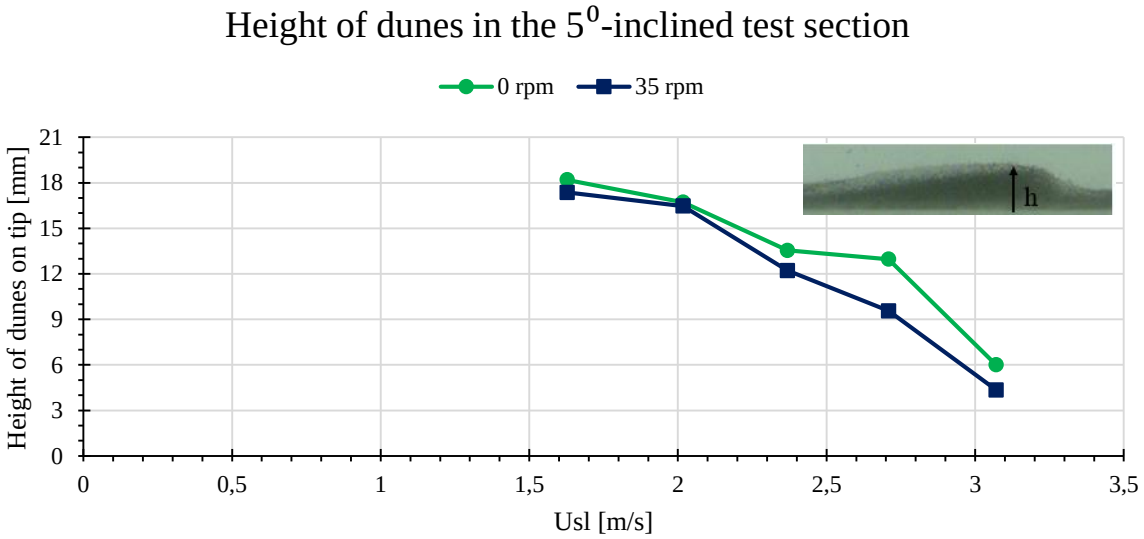

Figure 4.38: Height of dunes in two-phase flow for different Usl and rotation speed on the DS, the bumps indicates changes in flow patterns

Figure 4.38 shows the height of the dunes at different flow rates. The x-axis stands for Usl and y-axis for the measured height of the dunes. Figure 4.38 indicates higher dunes at 0 rpm. The curves shows bumps that indicates changes in flow patterns, the density on the top layer decreases and more particles are pushed up and making the bed height increasing.

It is not possible to compare figures 4.37 and 4.38 due to higher C_p when the DS was added. For higher rpm on the DS it was not possible to see settled particles at the bottom of the pipe. If we had used eccentricity of the pipe as a tool, we might have had settled particles when the pipe was on its way down. The eccentricity of the pipes makes an uncertainty on the height of the bed dunes.

5. Conclusion and further work

5.1. Conclusion

The main focus in this study was to investigate how different parameters affect the particle transport. Different experiments have been carried out to achieve new data showing the effects of inclination, flow rate, particle size and rotation of drill string. The differential pressure (DP), particles mass flow rate, velocity profiles of particle and liquid, and particle bed height were obtained by the use of the pressure transducers and the PIV and UVP measurement techniques. In this work, experimental analysis gave us significant results:

- The frictional pressure drop was found to be increased for small inclinations and even more at higher flow rates.
- By averaging the time series of raw data for DPs, the effect of rotational speed of DS disappeared on the presented DP for horizontal and 5°-inclined test section. The results for the 35°-inclined test section showed some influences on DP, but there was no logical tendency.
- The calculated particle mass flow rate from the collection system was increased exponentially to a certain liquid flow rate and was further increased linearly at higher liquid flow rates. The change of rotational speed of DS showed some small effects on particle collection rate.
- The particles transport in pipe inclination around 35° was determined to be the most difficult. In the pipe with 35°-inclination the particles were sliding backwards on the edge of the settling particles. This happened particularly at low flow rates.
- It was found that having different inclinations could affect the particle flow patterns. At higher inclination, the transition in flow patterns was occurring at lower superficial liquid velocity.
- The results of PIV and UVP were in good agreement and both detecting similar velocity profiles, even though there were some noises in the UVP data because of lack of seeding particles.
- Velocity profiles presented by the PIV gave information about the particles dynamic in pipe flow and were used to better describe the liquid-particle flow.
- It was challenging to define the flow patterns and transition in between by only doing personal visualization of the pipe flow. Using the recorded pictures helped us to

correctly identify the particles flow patterns. The results of that were in agreement with DP curves for horizontal and inclined test sections.

- At low liquid flow rates, the effect of rotation of DS was large. It caused the particles to be distributed more uniformly in the pipe cross section than when there was no rotation on DS. Rotation of DS resulted in higher efficiency on particle transport.

5.2. Future works

- In this study, Newtonian fluid was only utilized. It would be interesting to investigate the particle transportation using different rheology for drilling fluid i.e. non-Newtonian fluids.
- The characteristics on glass particles i.e. particle size, shape and overall concentration used in this thesis were not changing. Literature indicates that changing in characteristic affects the cuttings transport. Changes in size, shape and concentration would give a good indication on how large this effect is.
- Different rotation speed of DS in the 5°-inclined test section were investigated in this study. Change in angle of test section would give a good indication on whether the effect of rotating DS is constant or if it depends on the angle of pipe.
- PIV showed a good illustration of the particle dynamics and therefore recommended to use the velocity profile to identify the flow patterns at different flow rates.
- The study was performed purely experimental. It would be interesting to compare the results with parametric CFD studies or 3 layer modeling.

References

Adari, R. B., Miska, S., Kuru, E., Bern, P., & Saasen, A. (2000). *Selecting drilling fluid properties and flow rates for effective hole cleaning in high-angle and horizontal wells.* Paper presented at the SPE Annual Technical Conference and Exhibition.

Best, J., & Kostaschuk, R. (2002). An experimental study of turbulent flow over a low-angle dune. *Journal of Geophysical Research: Oceans (1978–2012), 107*(C9), 18-11-18-19.

Bilgesu, H. I., Mishra, N., & Ameri, S. (2007). *Understanding the effect of drilling parameters on hole cleaning in horizontal and deviated wellbores using computational fluid dynamics.* Paper presented at the Eastern Regional Meeting.

Brown, N. P. (1991). *Flow regimes of settling slurries in pipes*: Elsevier, London.

Clark, R., & Bickham, K. (1994). *A mechanistic model for cuttings transport.* Paper presented at the SPE Annual Technical Conference and Exhibition.

Crowe, C. T., Schwarzkopf, J. D., Sommerfeld, M., & Tsuji, Y. (2011). *Multiphase Flows with Droplets and Particles, Second Edition* (2nd ed. ed.). Hoboken: Taylor and Francis.

Doron, P., & Barnea, D. (1995). Pressure drop and limit deposit velocity for solid-liquid flow in pipes. *Chemical Engineering Science, 50*(10), 1595-1604. doi:10.1016/0009-2509(95)00024-Y

Doron, P., & Barnea, D. (1996). Flow pattern maps for solid-liquid flow in pipes. *International Journal of Multiphase Flow, 22*(2), 273-283.

Doron, P., Simkhis, M., & Barnea, D. (1997). Flow of solid-liquid mixtures in inclined pipes. *International Journal of Multiphase Flow, 23*(2), 313-323.

Duan, M., Miska, S., Yu, M., Takach, N. E., Ahmed, R. M., & Hallman, J. H. (2010). Experimental study and modeling of cuttings transport using foam with drillpipe rotation. *SPE Drilling & Completion, 25*(03), 352-362.

Egenti, N. B. (2014). *Understanding Drill-cuttings Transportation in Deviated and Horizontal Wells*.

Guney, M. S., Bombar, G., Aksoy, A. O., & Dogan, M. (2013). Use of UVP to investigate the evolution of bed configuration. *KSCE Journal of Civil Engineering, 17*(5), 1188-1197.

Haaland, S. E. (1983). Simple and explicit formulas for the friction factor in turbulent pipe flow. *Journal of Fluids Engineering, 105*(1), 89-90.

Hyun, C., Subhash, N. S., & Osisanya, S. O. (2000). *A Three-Segment Hydraulic Model for Cuttings Transport in Horizontal and Deviated Wells.* Paper presented at the SPE/CIM International Conference on Horizontal Well Technology.

Keane, R. D., & Adrian, R. J. (1992). Theory of cross-correlation analysis of PIV images. *Applied scientific research, 49*(3), 191-215.

Lazarus, J., & Neilson, I. (1978). *A generalized correlation for friction head losses of settling mixtures in horizontal smooth pipelines.* Paper presented at the Hydrotransport 5. Proc. 5th Int. Conf. on Hydraulic Transport of Solids in Pipes.

Li, J., & Walker, S. (2001). Sensitivity analysis of hole cleaning parameters in directional wells. *SPE Journal, 6*(04), 356-363.

Menge, B. K. (2015). *Analysis of Turbulent Flow in a Pipe at Constant Reynolds Number using Computational Fluid Dynamics.*

Mohammadsalehi, M., & Malekzadeh, N. (2011). *Optimization of hole cleaning and cutting removal in vertical, deviated and horizontal wells.* Paper presented at the SPE Asia Pacific Oil and Gas Conference and Exhibition.

Nazari, T., Hareland, G., & Azar, J. J. (2010). *Review of cuttings transport in directional well drilling: systematic approach.* Paper presented at the SPE Western Regional Meeting.

Neutrium. (Web-2012). Pressure loss i pipe. Retrieved from https://neutrium.net/fluid_flow/pressure-loss-in-pipe/

Okrajni, S., & Azar, J. (1986). The effects of mud rheology on annular hole cleaning in directional wells. *SPE Drilling Engineering, 1*(04), 297-308.

Rabenjafimanantsoa, A., Time, R. W., & Saasen, A. (2007). *Simultaneous UVP and PIV measurements related to bed dunes dynamics and turbulence structures in circular pipes.* Paper presented at the 5th International Symposium on Ultrasonic Doppler Methods for Fluid Mechanics and Fluid Engineering.

Rabenjafimanantsoa, H. (2007). *Particle transport and dynamics in turbulent newtonian and nonnewtonian fluids.* PhD Thesis, U. of Stavanger, Stavanger.

Rabenjafimanantsoa, H. A., Time, R. W., & Saasen, A. (2005). Flow regimes over particle beds : experimental studies of particle transport in horizontal pipes. [S.l.]: The Nordic Theology Society, 2005.

RheoSense. (Web-2016). Viscosity of Newtonian and non-Newtonian Fluids. Retrieved from http://www.rheosense.com/applications/viscosity/newtonian-non-newtonian

Shook, C. A., & Roco, M. C. (1991). *Slurry flow : principles and practice*. Boston: Butterworth-Heinemann.

Takeda, Y. (1999). Ultrasonic Doppler method for velocity profile measurement in fluid dynamics and fluid engineering. *Experiments in fluids, 26*(3), 177-178.

Thielicke, W., & Stamhuis, E. (2014). PIVlab–Towards user-friendly, affordable and accurate digital particle image velocimetry in MATLAB. *Journal of Open Research Software, 2*(1).

Turian, R. M., & Yuan, T. F. (1977). Flow of slurries in pipelines. *AIChE Journal, 23*(3), 232-243.

Walker, S., & Li, J. (2000). *The effects of particle size, fluid rheology, and pipe eccentricity on cuttings transport.* Paper presented at the SPE/ICoTA Coiled Tubing Roundtable.

Appendix

Appendix A: MATLAB scripts

A.1: Calculating the average values out from the measurements

```
% Program for calculating the average measurements in the test sections


clc
clear
close all;
RESULTS = [];

% Constant values

d = 40/1000;                              %pipe diameter m
L_H = 1.52;          %unit m              %Distance between two tap pressure
L_5 = 1.52;          %unit m              %Distance between two tap pressure
L_40 = 0.60;         %unit m              %Distance between two tap pressure
L_bend = 0.57;       %unit m              %Distance between two tap pressure
E =402102;            %row number of the last data in the excel sheet
S=3;                  %row number of the first data in the excel sheet
% Reading excel file (from Data Acquisition)

% Excel name
filename = 'Water Calibration Testpiv1403';

% number of sheets in the excel file
i=10;

% Define sheet name
sheet=strcat('f',num2str(i));
% Scanning the excel file
[NUM,TXT,RAW] = xlsread(filename,sheet);
val = NUM;

% Computing variables (Mass Flow rate, Density, Usl, Dp-H, Dp-5 degree,
% Dp-40 degree, Dp-Bend (90 degree)

mfr = mean(val(S:E,6))/3600;         %unit (kg/s)
den = mean(val(S:E,7))*1000;         %unit (kg/m^3)
Usl = mfr/(den*pi()*d^2/4);              %unit (m/s)
DP_h = mean(val(S:E,2)) /1.52;       %unit (mpa/m)
DP_5 = mean(val(S:E,4))/1.52;        %unit (mpa/m)
DP_40 = mean(val(S:E,3)) /0.6;       %unit (mpa/m)
DP_bend = mean(val(S:E,5)) /0.57;      %unit (mpa/m)

% Min and Max
DP_hmin = min(val(S:E,2)) /1.52;       %unit (mpa/m)
DP_hmax = max(val(S:E,2)) /1.52;       %unit (mpa/m)
DP_5min = min(val(S:E,4))/1.52;        %unit (mpa/m)
DP_5max = max(val(S:E,4))/1.52;        %unit (mpa/m)
DP_40min = min(val(S:E,3)) /0.6;       %unit (mpa/m)
DP_40max = max(val(S:E,3)) /0.6;       %unit (mpa/m)
```

```
DP_bendmin = min(val(S:E,5)) /0.57;      %unit (mpa/m)
DP_bendmax = max(val(S:E,5)) /0.57;      %unit (mpa/m)

%LowPass Fillter
val_mfr = smooth(val(S:E,6));
val_den = smooth(val(S:E,7));
val_DP_h = smooth(val(S:E,2))/1.52;
val_DP_5 = smooth(val(S:E,4))/1.52;
val_DP_40 = smooth(val(S:E,3))/0.60;
val_DP_bend = smooth(val(S:E,5))/0.57;

% Plot
figure;
s(1) = subplot(3,2,1);
s(2) = subplot(3,2,2);
s(3) = subplot(3,2,3);
s(4) = subplot(3,2,4);
s(5) = subplot(3,2,5);
s(6) = subplot(3,2,6);

plot(s(1),val(S:E,1),val_mfr);
title(s(1),'Mass flow rate')
xlabel(s(1),'Time [s]','FontSize',14);
ylabel(s(1),'Mass flow rate [kg/s]','FontSize',14);

plot(s(2),val(S:E,1),val_den);
title(s(2),'Density')
xlabel(s(2),'Time [s]','FontSize',14);
ylabel(s(2),'Density [kg/m^3]','FontSize',14);

plot(s(3),val(S:E,1),val_DP_h);
title(s(3),'Differential Pressure - Horizontal')
xlabel(s(3),'Time [s]','FontSize',14);
ylabel(s(3),'DP/L [mpa/m]','FontSize',14);

plot(s(4),val(S:E,1),val_DP_5);
title(s(4),'Differential Pressure - 5 Degree')
xlabel(s(4),'Time [s]','FontSize',14);
ylabel(s(4),'DP/L [mpa/m]','FontSize',14);

plot(s(5),val(S:E,1),val_DP_40);
title(s(5),'Differential Pressure - 40 Degree')
xlabel(s(5),'Time [s]','FontSize',14);
ylabel(s(5),'DP/L [mpa/m]','FontSize',14);

plot(s(6),val(S:E,1),val_DP_bend);
title(s(6),'Differential Pressure - Bend')
xlabel(s(6),'Time [s]','FontSize',14);
ylabel(s(6),'DP/L [mpa/m]','FontSize',14);

%write the results in a vector
RESULTS = [RESULTS; mfr, den, Usl, DP_h,DP_5,DP_40,DP_bend]
minandmax =
[DP_hmin,DP_hmax,DP_5min,DP_5max,DP_40min,DP_40max,DP_bendmin,DP_bendmax]
```

A.2: Converting rgb images to gray images

```
clc
clear all
for i = 100:1:100
    close all
    N{i}=strcat('acA800-
510uc__21763334__20160218_122055750_0',num2str(i),'.tiff');
%pictures need to have the numbers as name
    I1 = imread(N{i});
    I1=rgb2gray(I1);
    %figure('name','original_image','numbertitle','off'), imshow(I1);
    imwrite(I1,['00' , int2str(i) , '.bmp'],'bmp');
        end
```